An experimental method of measuring the confined compression strength of geomaterials

P. Forquin [a,*], A. Arias [b], R. Zaera [b]

[a] *Laboratory of Physics and Mechanics of Materials, UMR CNRS 75 54, University of Metz, Ile du Saulcy, 57045 Metz cedex, France*
[b] *Department of Continuum Mechanics and Structural Analysis, University Carlos III of Madrid, Avda. de la Universidad 30, 28911, Leganés, Madrid, Spain*

Abstract

Knowledge of the behaviour of geomaterials under confined compression is a pre-requisite for any analysis of their ballistic performance. This study proposes an experimental method of determining the spherical and deviatoric behaviour of these materials under high pressure. Known as the 'quasi-oedometric compression test' it consists of compressing a cylindrical specimen tightly enclosed in a thick confinement vessel. The principles of these quasi-oedometric tests are given first, and the steps taken for their execution, together with an examination of the steel used for the confinement vessel. An original way of analysing the data of the test is presented and validated by numerical simulations. These calculations provide valuable information about the influence of the interface product introduced between the vessel and the specimen, and that of friction. Tests are then presented with specimens of aluminium alloy to validate the experimental set-up and the method of analysis. In addition, quasi-oedometric compression tests of cement based material, with and without particles, illustrate the opportunities offered by this testing method, and show that its deviatoric strength and compaction law are significantly improved by ceramic granulates addition.

Keywords: Concrete; Metallic materials; Constitutive behaviour; Mechanical testing; Quasi oedometric compression tests

1. Introduction

A good grasp of the behaviour of geomaterials under confined compression is essential to any understanding and modeling of their ballistic performance. In the impact of a projectile on a massive target, a field of confined compression is created ahead of the projectile. The resistance of the material under high pressure, the law of compaction (irreversible diminution of the volume) and (to a lesser extent in geomaterials) the elastic parameters, will condition the penetration of the projectile into the target (Hanchak et al., 1992; Xu et al., 1997; Yankelevsky and Dancygier, 2001), and this is why confined compression tests have been developed. We now proceed to consider their principles and their drawbacks.

* Corresponding author. Tel.: +33 3 87 54 72 49; fax: +33 3 87 31 53 66.
E mail address: forquin@univ metz.fr (P. Forquin).

Triaxial compression tests provide a measurement of the strength of geomaterials at different confinement pressures. A purely hydrostatic pressure is applied on a cylindrical specimen, and this is followed by axial compression. The strength, in Mises sense, is taken as the maximum axial stress on withdrawal of the pressure exerted by the confinement fluid. These tests have been carried out for several decades on concretes (Palaniswamy and Shah, 1974), on rocks (Hoek and Franklin, 1968; Cagnoux and Don, 1994) (limestone and quartzite), and on ceramics (Heard and Cline, 1980) (alumina-type ceramics, aluminium nitride, and beryllium or magnesium oxide). All these reports state that materials known for their brittle or quasi-brittle behaviour under uniaxial compression undergo a change to ductile behaviour under high pressure confinement. One point to be noticed is that when the axial strain is exceeding about 1–2%, the stress difference is reaching a threshold and is kept roughly constant while the axial strain is increasing up to 6–10% (this point corresponding usually to a localisation of the deformation within the specimen). This behaviour was observed in ceramic materials (Heard and Cline, 1980) as well as in rocks (Cagnoux and Don, 1994) and concrete materials (Kotsovos and Newman, 1980; Xie et al., 1995; Bažant et al., 1996; Buzaud, 1998) for a wide range of hydrostatic pressures above a few 10 MPa. Therefore, the strength of concretes is thought to be pressure-dependant and strain-independent as a first approximation. As explained latter, this assumption will be necessary to deduce the confined behaviour of concrete materials from a single quasi-oedometric compression test.

Finally, triaxial tests reveal the behaviour of geomaterials under high pressure but they are not without limitations and difficulties; they demand a very high pressure chamber (100–1000 MPa) coupled to a load frame (Wallace and Olden, 1965) and they require impermeability between the fluid and the specimen that can be difficult to achieve, so they are not easy to carry out.

Compression tests known as quasi-oedometric can also be done on geomaterials (their name refers to the very weak radial displacement during the test). A cylindrical concrete specimen is placed in a confinement vessel. Under axial compression, the specimen tends to expand under the effect of radial dilatancy and presses against the confinement vessel. In the course of the test we observed a rise of both the axial and the radial stresses in the specimen, so the hydrostatic confinement pressure varies considerably and this gives us a reading of the strength at different levels of the pressure.

However, since the test is driven only by the axial strain, it does not show whether the variations of the strength are mainly due to a rise of the confinement pressure or whether it is an effect of the increase of axial strain. In other words, a quasi-oedometric compression test reveals the evolution of strength of the material for one loading path (i.e., the oedometric loading path) for which the state of strain (axial or shear) and hydrostatic pressure is changing. It does not say whether the variation of the strength is provoked mainly by the variation of the strain or by that of the hydrostatic pressure and if it might be changed through a different loading path. So if the test is intended to identify the parameters of a constitutive model, this distinction must be made clear. For example, we present quasi-oedometric compression tests carried out with aluminium and with concrete. In the first group, the test shows the evolution of the strength with the deviatoric strain, assuming no influence of pressure. In the second, the results are expressed by a diagram strength/hydrostatic pressure, assuming no influence of the variation of strain under a constant pressure. If this hypothesis of decoupling of pressure and strain is not plausible or if the behaviour is depending of loading path, it means that a single oedometric compression test cannot provide a complete identification. It could serve only to validate a model of behaviour identified by other means, such as by multiple triaxial compression tests.

Several experimental devices for quasi-oedometric compression were set up by Bažant et al. (1986), Burlion (1997) and Gatuingt (1999). It was Burlion (1997) who first devised an instrumented vessel of 53 mm interior diameter and 140 mm exterior diameter, considered stressed in its elastic domain. An interface product introduced between the vessel and the specimen at the moment of inserting the latter ensures a correction of any possible defects of cylindricality, parallelism or flatness, and coaxiality of the surfaces of the specimen. The interface product is an epoxy bi-component resin, Chrysor® C6120, commonly used for structural applications, and once polymerized, eliminates any internal gap. The radial strain and the radial stress of the specimen were deduced from the micro-deformation of the vessel (some hundredths of %) by means of gauges attached to the outer surface of the vessel (Burlion et al., 2001). In the analysis it is assumed on one hand that the vessel is always in its elastic domain, and on the other that the interface product is incompressible and that friction is negligible between the vessel and the specimen (Burlion et al., 2001). Moreover, the well-known ana-

lytical solution of an elastic tube subjected to a uniform pressure applied against the inner wall of the tube was used to deduce the radial stress and strain within the specimen. So, the axial contraction of the specimen (i.e., its average axial strain) and the 'barrel' deformation of the vessel were not taken into account in this analysis. Two smaller vessels were used to test MB50 micro-concrete (50 mm long, 30 or 50 mm interior diameter, and 50 or 70 mm exterior diameter) (Gatuingt, 1999). They had the advantage of being usable with Hopkinson bar device (Kolsky, 1949). The small thickness of the vessel ensured more sensitivity of the gauges attached to the vessel. Gatuingt (1999) reported a strong hardening of the material followed by a saturation of the axial stress at around 900 MPa. The axial strain might reach −30% before unloading. In addition, a numerical method was proposed for the evaluation of the radial stress in the specimen from the hoop strain measured on the outer surface of the vessel (Forquin, 2003). This was applied to the quasi-static and dynamic tests performed by Gatuingt. The analysis showed a very limited influence of the rate of loading on the strength, even at a strain rate that reached 400 s^{-1} (Forquin, 2003). In this paper, a new methodology is proposed and implemented to analyse the behaviour of materials under quasi-oedometric compression tests. Improvements concern in one hand the taking into account of the plastic deformation of the vessel, its 'barrel' deformation and the axial contraction of the specimen. On the other hand, numerical simulations are conducted to underline the influence of friction, Chrysor® interface product and a potential vacuum in the vessel. Moreover, a "reference" material is used to evaluate the possible scatter of this testing methodology.

2. Principle of the quasi-oedometric compression test

The diagram of Fig. 1 explains the functioning of the quasi-oedometric compression tests carried out in the course of this study. The specimen enclosed in the confinement vessel is subjected to axial compression applied by the universal testing machine (Servosis®). The axial stress in the specimen can be deduced from the load cell. In addition, an analog extensometer is placed between the two compression cylinders. This instrumentation gives the axial strain of the specimen on withdrawal of the displacement caused by the elastic axial strain of the compression cylinders. Four strain gauges are attached to the confinement vessel; we now present their position and their function.

In Fig. 2 we see the universal testing machine used for the tests. The maximum load reached in the confined compression test is about 750 kN, fairly close to the maximum operating capacity of the machine. For this reason, the concrete specimens used in this study are not more than 30 mm in diameter. Fig. 3 illustrates the set-up for the triaxial compression: a confinement vessel fitted with gauges and round compression plates on platforms. The extensometer for measuring the axial strain is attached to compression cylinders by filleted screws screwed to the flasks. The system provides a close alignment of the screws and ensures that the extensometer held perfectly vertical. The vessel is filled by Chrysor® product before the specimen introduction. Therefore, when the specimen attached to the top bar is inserted, the Chrysor® product is pushed out or is spreading out at the interface between the specimen and the vessel.

The steel confinement vessel is a crown of about 30 mm interior diameter, 55 mm outer diameter and 46 mm long. The outer diameter was chosen as a compromise between a sufficient stiffness of the vessel (diameter large enough) and a good sensibility of strains measurement on the external surface of the vessel (diameter small enough). Concerning the length of the crown, it was chosen a little greater than that of the cylindrical specimen (about 40 mm) to ensure better airtightness between the compression cylinders and the vessel, espe-

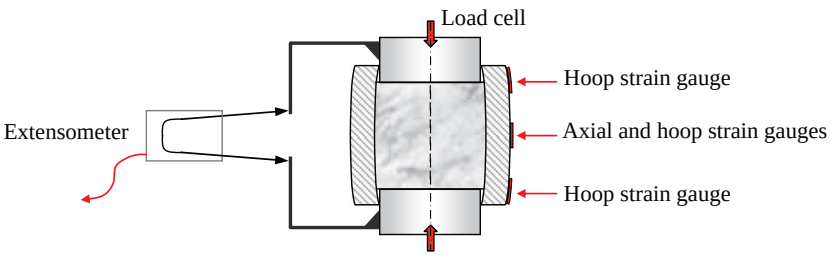

Fig. 1. Sketch of the quasi oedometric compression test set up.

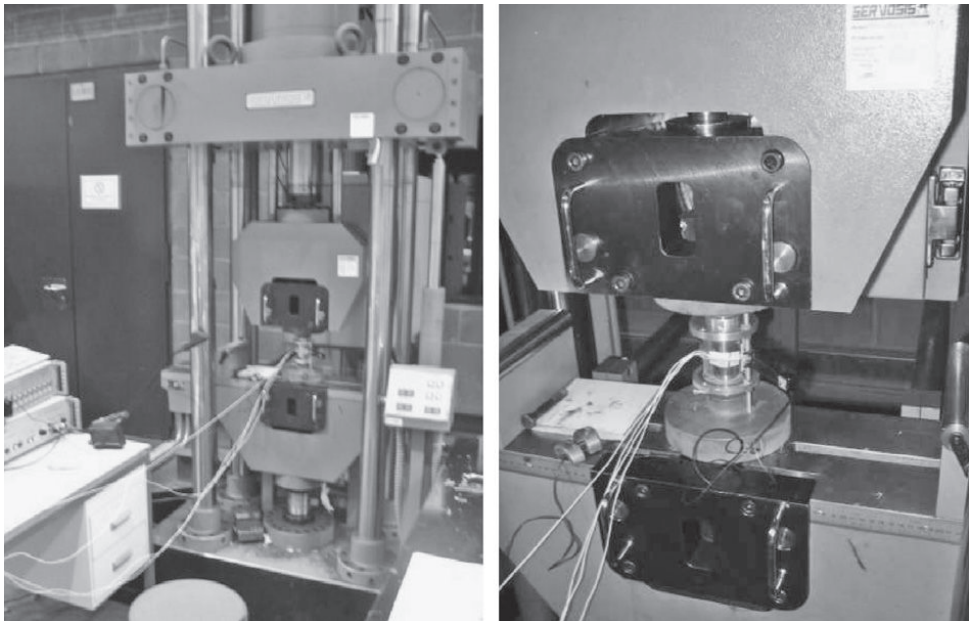

Fig. 2. Thousand kiloNewtons universal testing machine Servosis® used for the tests.

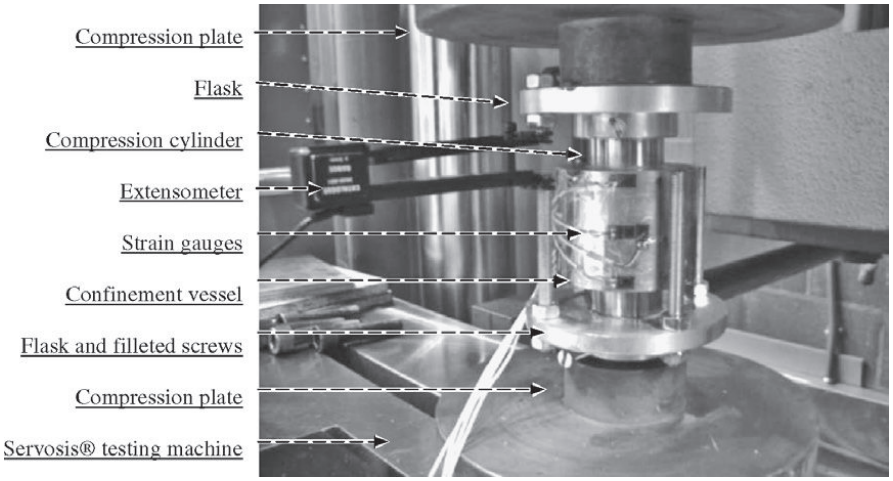

Fig. 3. Picture of the experimental set up for the quasi oedometric compression test.

cially at the moment of extruding the Chrysor® polymer. The deformation of the vessel is heterogeneous, and the expansion is registered by the three hoop strain gauges attached around the surface of the vessel, one at the level of the symmetry plane and the other two at a distance of 18 mm from this level. The axial gauge on the symmetry plane allows controlling the barrelling of the vessel.

3. Proposal and validation of a new method of analysis of quasi-oedometric compression tests

To estimate the evolution of the strength of a specimen, one must know the lateral pressure applied by the specimen on the inner wall of the vessel. We consider first the plastic behaviour of the steel of the vessel, and present a method of estimating the radial stress applied on the inner wall of the vessel and the radial internal strain as a function of the external hoop strain. This method is validated by a series of numerical simulations of the quasi-oedometric compression test with aluminium alloy specimens. These simulations show the influence of the behaviour of the vessel and that of any possible friction between the surfaces in contact. They also

demonstrate the possible role of the interface product Chrysor®. Once validated this method of data analysis, it is applied to the quasi-static quasi-oedometric compression tests performed with aluminium specimens.

3.1. Behaviour of the steel of the vessel

The confinement vessel is of stainless steel AISI 316. All the vessels and all the tension samples were obtained from a single steel bar 1 m long and 55 mm diameter. Two tension samples were cut from the centre of the bar and tested by means of a 100 kN Instron® machine. The strain was measured by an extensometer or by a gauge attached to the specimen. The axial stress is plotted on Fig. 4 versus the plastic strain corresponding to total logarithmic axial strain minus the elastic axial strain. The two tests give the same result.

As a check on the homogeneity of the steel bar, Vickers HV10 hardness tests (10 N) were done on the tension samples before testing and on one confinement vessel. The various measurements of the specimens gave a hardness of 171 ± 2 (HV10). Those of the vessel are shown in the diagram of Fig. 5. Five lines of measurement, each at 13 points, show very good reproducibility of the measurement for a given angle and radius, but also a weak influence of the angle of the measured line and a strong influence of the radius. So the field of hardness is axisymmetric and the hardness increases sharply with the radius. The hardness can be arranged into 3 zones: the first close to the outer surface with a hardness rating of 290; the second between 18 and 24 mm with a rating of 273, and the third at a radius below 18 mm. Heterogeneity of hardness field is certainly the consequence of the processing of the bar (extrusion process, surface treatment). From these measurements it is clear that the behaviour of the steel cannot be identified from a sample taken from the centre of a bar. That's why additional tests were therefore performed with flat specimens taken from a confinement vessel. Their positions are shown in Fig. 6.

Samples 1 and 2 are taken from between r 15 and r 18 mm; numbers 4 and 6 from between 18 and 21 mm; nos. 5 and 7 between 21 and 24 mm of the axis of the vessel. Specimens 3 and 8 are the farthest away (24 and 27 mm) from the centre. The specimens are flat, of cross section 3×6 mm^2. No slipping of the samples was detected during the tests, in spite of the large axial strains observed. The axial strain was measured by means of an extensometer placed in the central part of the samples. The results of the tensile tests are shown in Fig. 6. Of special interest is the fact that the plastic behaviour remains unaffected by unloadings/reloadings.

The behaviour of the samples from fully inside the thickness of the vessel – specimens 4, 5, 6, and 7 – is very similar, whereas that of the E8 shows a very high yield stress ($\sigma_{y0,2} \approx 640$ MPa), much higher than that of the

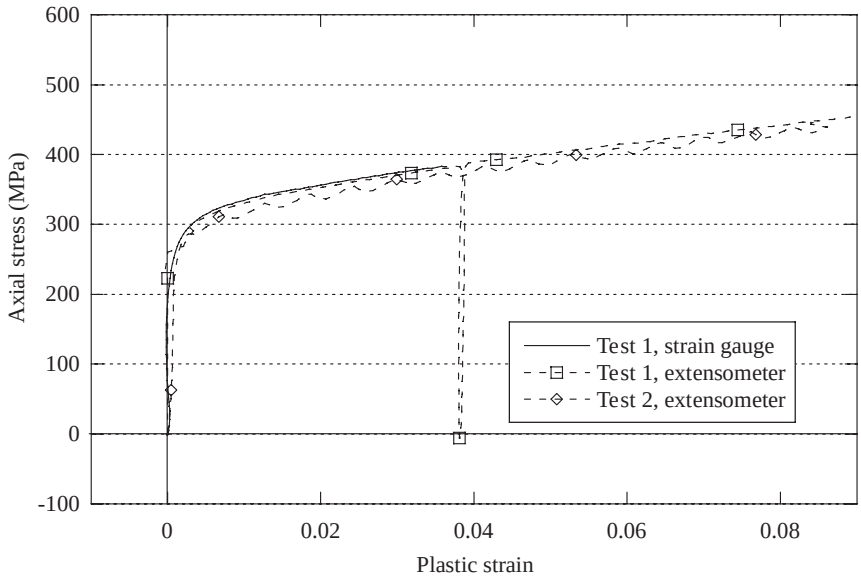

Fig. 4. Tensile tests performed on two specimens cut from the centre of the steel bar.

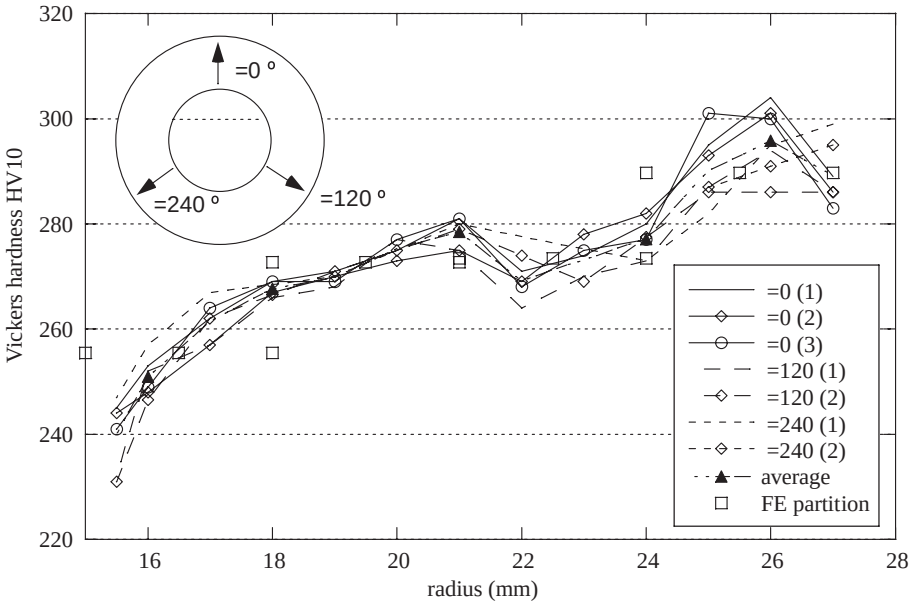

Fig. 5. Profile of Vickers HV10 hardness along the radius of the confinement vessel at different angles.

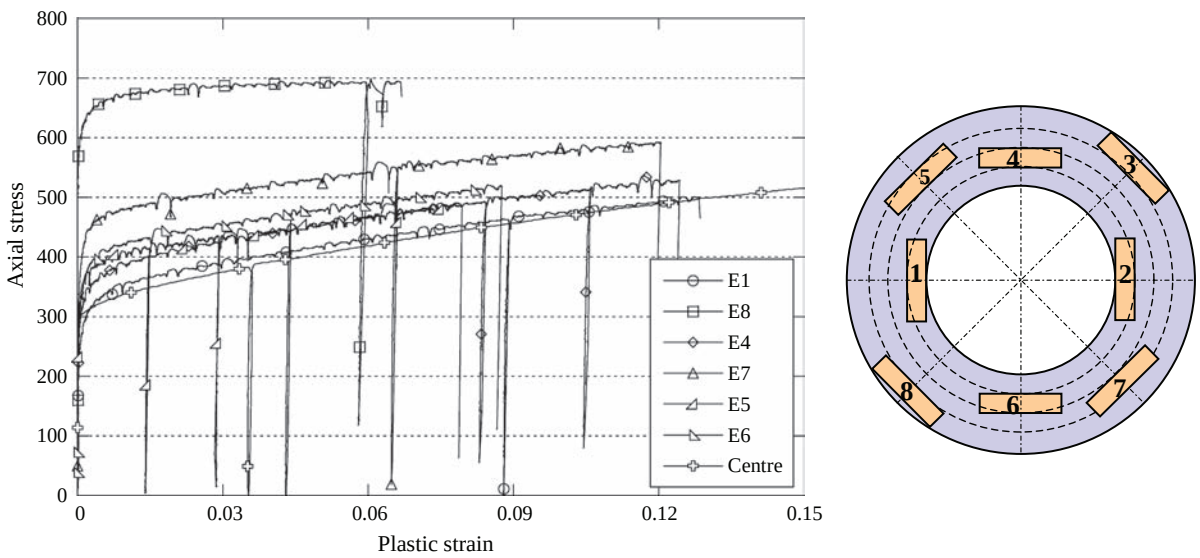

Fig. 6. Results of the tensile tests along the radius of the confinement vessel (axial stress versus plastic strain).

sample E1 at a radius of 16.5 mm ($\sigma_{y0,2} \approx 300$ MPa). The behaviour of E1 is very close to that of the samples taken from the centre of the bar (Fig. 4). The curves in Fig. 6 allowed the identification of the strain hardening of samples from E1 to E8 within the strain range 0–10%. These curves are correctly described by values given in Table 1. The average stresses of samples 4 and 6 and of 5 and 7 is also given in this table.

The high hardening observed favours the use of this steel as the material of the confinement vessel. The low yield stress raises its sensitivity to strain under low internal pressures, and the high strength imposes a limit to the radial strain of the concrete and a state close to that of uniaxial strain. In addition, a higher global stiffness of the vessel favours an exploration of the behaviour of the concrete over a wider range of confinement pressure. The high failure strain prevents any localisation of the deformation in the vessel during the tests.

Table 1
Plastic behaviour of the samples of AISI 316 steel tested between 0% and 10% plastic strain

Plastic strain	σ (E1) (MPa)	σ (E4) (MPa)	σ (E6) (MPa)	Average of 4 and 6	σ (E5) (MPa)	σ (E7) (MPa)	Average of 5 and 7	σ (E8) (MPa)
0	170	190	200	195	200	240	220	523
0.0003	233	272	290	281	290	346	318	580
0.001	273	316	356	336	340	406	373	617
0.002	305	348	380	364	374	444	409	640
0.008	354	384	422	403	404	480	442	674
0.03	394	429	455	442	434	508	471	686
0.06	430	470	490	480	469	543	506	694
0.1	475	510	530	520	510	582	546	700

3.2. Global behaviour of the vessels used in the tests

The aim is to deduce, from measurement of the hoop strain of the exterior of the vessel, the average internal pressure brought to bear on the walls of the vessel by the specimen. This can be deduced from a numerical simulation that takes into account the elastoplastic behaviour of the material of the vessel (Forquin, 2003). Two simulations were done with the implicit finite element code Abaqus (Hibbitt et al., 2003). We used 4-node axisymmetric elements (CAX4 in ABAQUS notation).

The vessel is a cylindrical crown of 55 mm external diameter, 30.4 mm inside diameter and 43 mm height and is composed in the FE simulations of four layers modelled by an elastoplastic behaviour which hardening law is one of those of Table 1. In the first simulation, a radial compression is exerted on the inner cylindrical surface of the vessel, to a height of 40 mm, and in the second to a height of 34 mm. By comparing the two calculations, the effect of the height of the zone of application of the radial stress is evaluated, and the height of this zone reflects the axial contraction of the specimen. In addition, this axial contraction (the average axial strain of the specimen) is measured directly. The results of the two numerical simulations are given in Figs. 7–10.

From Figs. 7 and 8, one can deduce the evolution of the average interior radial stress $\sigma_{\text{radial}} = \sigma_{rr}^{(r=15)}$ as a function of the external hoop strain $\varepsilon_{\theta\theta}^{(z=0,\text{ext})} = \varepsilon_{\theta\theta}(z = 0, r = 27.5\ \text{mm})$ in which z is the scale in the axial direc-

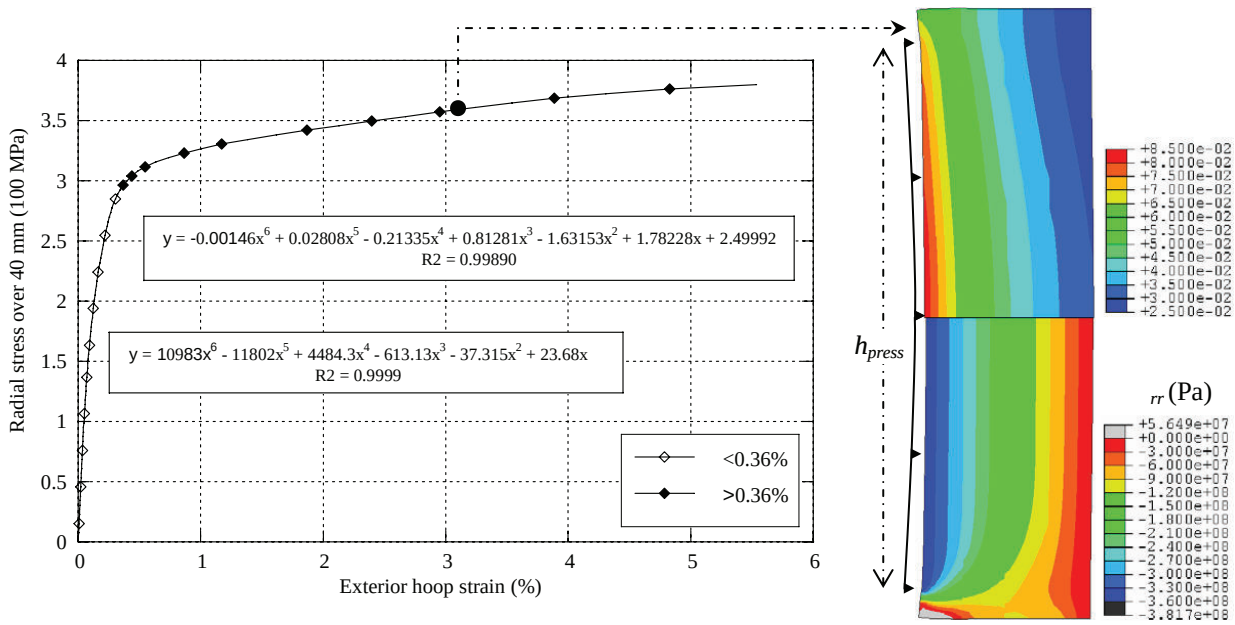

Fig. 7. Numerical simulation of a vessel subjected to a scale of pressure of 0 400 MPa to a height h_{press} of 40 mm on its inner surface. Determination of $\sigma_{rr} = f_{40}(\varepsilon_{\theta\theta})$ function.

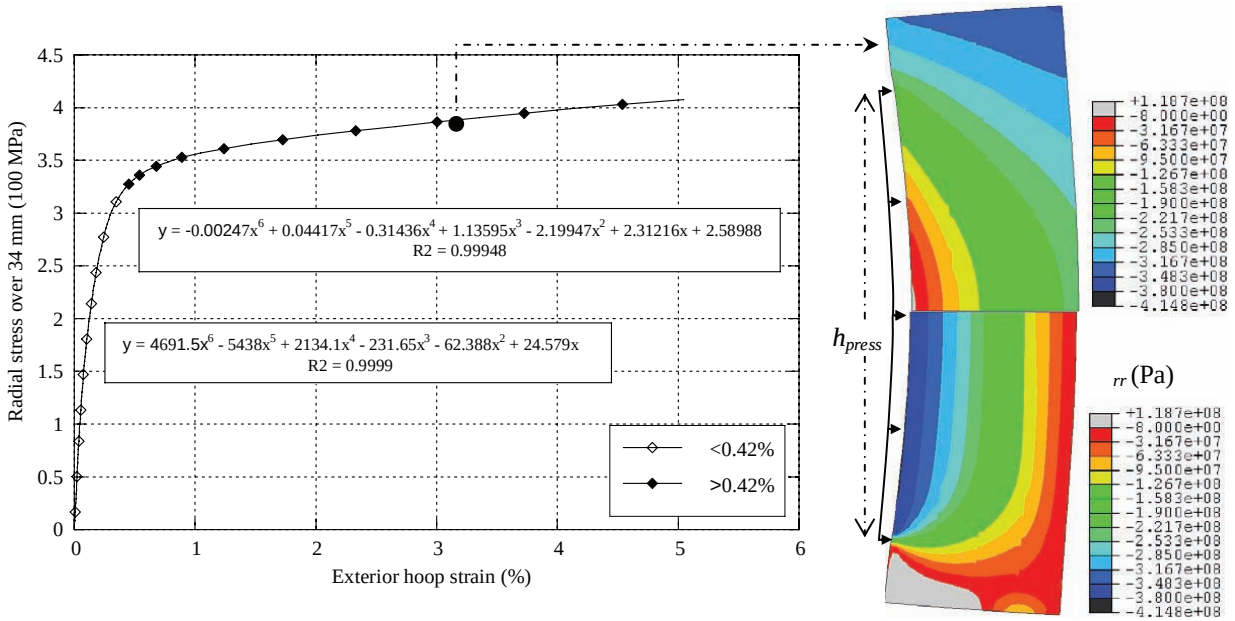

Fig. 8. Numerical simulation of a vessel subjected to a scale of pressure of 0 400 MPa to a height h_{press} of 34 mm on its inner surface. Determination of $\sigma_{rr} = f_{34}(\varepsilon_{\theta\theta})$ function.

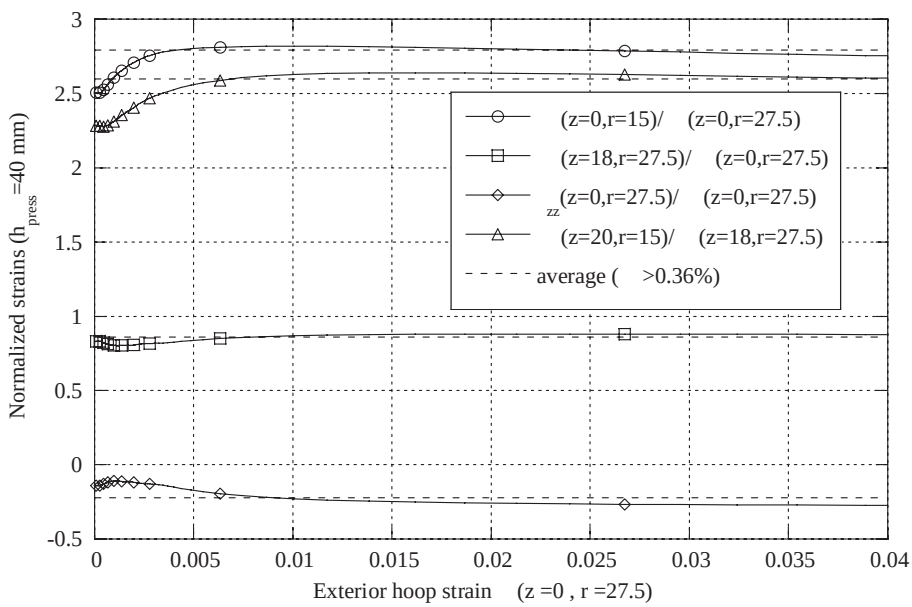

Fig. 9. Evolution of the internal hoop strains at $z = 0$ and 20 mm, and of the outer axial strain as a function of the external hoop strain at $z = 0$. Internal pressure over 40 mm height.

tion and z 0 the origin of the horizontal symmetry. The height of 34 mm allows the specimen/vessel contact to be taken as a nominal 15% axial strain. The internal radial stress is assumed to be given by the linear equation

$$-\sigma_{\text{radial}}\left(\varepsilon_{\text{axial}}, \varepsilon_{\theta\theta}^{(z\ \ 0,\text{ext})}\right) = \left(1 - \frac{\varepsilon_{\text{axial}}}{\varepsilon_{\text{ref}}}\right) f_{40}\left(\varepsilon_{\theta\theta}^{(z\ \ 0,\text{ext})}\right) + \left(\frac{\varepsilon_{\text{axial}}}{\varepsilon_{\text{ref}}}\right) f_{34}\left(\varepsilon_{\theta\theta}^{(z\ \ 0,\text{ext})}\right) \tag{1}$$

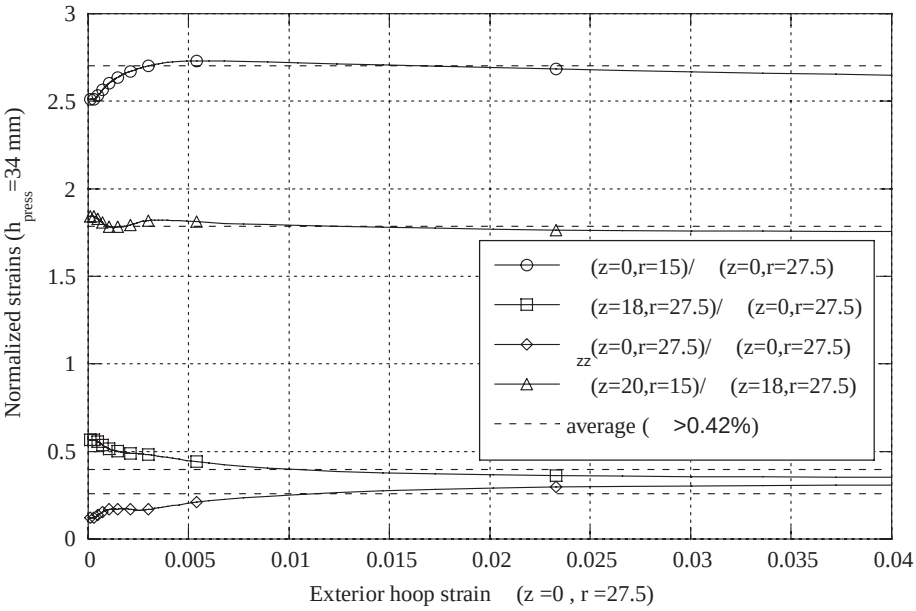

Fig. 10. Evolution of the internal hoop strains at $z = 0$ and 20 mm, and of the outer axial strain as a function of the external hoop strain at $z = 0$. Internal pressure over 34 mm height.

in which $\varepsilon_{\text{axial}}$ is the nominal axial strain of the specimen, ε_{ref} the reference strain (ε_{ref} -0.15), and $f_{40}(\varepsilon_{\theta\theta}^{(z=0,\text{ext})})$, $f_{34}(\varepsilon_{\theta\theta}^{(z=0,\text{ext})})$ are the functions identified in Figs. 7 and 8. One may ask whether a linear interpolation between f_{40} and f_{34} is a reasonable approximation. In fact, Figs. 7 and 8 show that the relative gap between the two functions f_{40} and f_{34} is quite small (less than 10%) and the lateral pressure is about 40% of the axial stress. Therefore, a linear interpolation is a possible approximation if the axial strain does not exceed the reference strain. This condition was always fulfilled for the tests performed in this study. Moreover, numerical simulations of quasi-oedometric compression tests were developed that allows to compare the lateral force given by the FE code and that obtained average from the radial stress given by Eq. (1). The difference was less than 5% if axial strain did not exceed 15%.

In the same way, Figs. 9 and 10 show the evolution of the internal hoop strains (r 15 mm, z 0–20 mm) $\varepsilon_{\theta\theta}^{(z=0,\text{int})}$ and $\varepsilon_{\theta\theta}^{(z=20\ \text{mm},\text{int})}$ as a function of the external hoop strains ($\varepsilon_{\theta\theta}^{(z=0,\text{ext})}$, $\varepsilon_{\theta\theta}^{(z=18,\text{ext})}$) on account of the internal radial stress applied on a height h_{press} of 34 and of 40 mm. These two strains are measured during the tests. The internal hoop strains are practically proportional to the external ones ($\varepsilon_{\theta\theta}^{(z=0,\text{ext})}$, $\varepsilon_{\theta\theta}^{(z=18,\text{ext})}$). The coefficient of proportionality (α_0^0,α_{20}^{18}), calculated by averaging over a range of the hoop external strain between 0.36% or 0.42% and 4%, is given in Table 2.

To calculate the average radial strain on the specimen $\varepsilon_{\text{radial}}$, a 'barrel' deformation of the vessel may be assumed, of the type $U_r(z) = U_r^{(z=0)} + (U_r^{(z=h/2)} - U_r^{(z=0)}) \cdot (2z/h)^2$ and under this hypothesis the average radial strain of the specimen is expressed by

$$\varepsilon_{\text{radial}} = \frac{2}{3}\varepsilon_{\theta\theta}^{(z=0,\text{int})} + \frac{1}{3}\varepsilon_{\theta\theta}^{(z=\frac{h}{2}\ \ U_{\text{axial,int}})} \tag{2}$$

and thus

Table 2
Average internal hoop strain at $z = 0$ and 20 mm from the horizontal symmetry plane

Average over $\varepsilon_{\theta\theta} \in (0.36\%\ \ 0.42\%;\ 4\%)$	$\varepsilon_{\theta\theta}^{(z\ \ 0,r\ \ 15)}/\varepsilon_{\theta\theta}^{(z\ \ 0,r\ \ 27,5)}$	$\varepsilon_{\theta\theta}^{(z\ \ 20,r\ \ 15)}/\varepsilon_{\theta\theta}^{(z\ \ 18,r\ \ 27,5)}$	$\varepsilon_{\theta\theta}^{(z\ \ 18,r\ \ 27,5)}/\varepsilon_{\theta\theta}^{(z\ \ 0,r\ \ 27,5)}$	$\varepsilon_{zz}^{(z\ \ 0,r\ \ 27,5)}/\varepsilon_{\theta\theta}^{(z\ \ 0,r\ \ 27,5)}$
$h_{\text{press}} = 40$ mm	2.79	2.60	0.86	0.22
$h_{\text{press}} = 34$ mm	2.70	1.79	0.40	0.26
Identification	α_0^0 2.745	α_{20}^{18} 2.20	0.63	

$$\varepsilon_{\text{radial}} = \frac{2}{3}\left(1 - \varepsilon_{\text{axial}}\left(1 + \frac{\varepsilon_{\text{axial}}}{2}\right)\right)\alpha_0^0 \varepsilon_{\theta\theta}^{(z=0,\text{ext})} + \frac{(1+\varepsilon_{\text{axial}})^2}{3}\alpha_{20}^{18}\varepsilon_{\theta\theta}^{(z=18,\text{ext})}. \tag{3}$$

Since the average radial strain and the average radial stress in the specimen are known, one can deduce the average axial stress as well as the deviatoric stress (in this case: $\sigma_{\text{deviatoric}} = \sigma_{\text{von Mises}}$) and the hydrostatic pressure

$$\sigma_{\text{axial}} = f(F_{\text{axial}}, \varepsilon_{\text{radial}}), \tag{4}$$

$$\sigma_{\text{deviatoric}} = |\sigma_{\text{axial}} - \sigma_{\text{radial}}|, \tag{5}$$

$$P_{\text{hydrostatic}} = -\frac{1}{3}(\sigma_{\text{axial}} + 2\sigma_{\text{radial}}), \tag{6}$$

the equivalent and volumetric strains being given by the formulae

$$\varepsilon_{\text{equivalent}} = \frac{2}{3}|\ln(1+\varepsilon_{\text{axial}}) - \varepsilon_{\text{radial}}|, \tag{7}$$

$$\varepsilon_{\text{volumetric}} = (1+\varepsilon_{\text{axial}})(1+\varepsilon_{\text{radial}})^2 - 1. \tag{8}$$

Then, knowing the axial force, the axial strain, and the exterior hoop strain measured by two gauges attached to the vessel; from these Eqs. (2)–(6) we can determine the deviatoric behaviour (i.e., the evolution of the deviatoric stress) and the spherical behaviour (the variation of the volumetric strain with the hydrostatic pressure). Summarizing, Fig. 11 sketches the process to obtain the needed variables averaged over the specimen σ_{axial}, σ_{radial}, $\varepsilon_{\text{axial}}$, and $\varepsilon_{\text{radial}}$ from the measurements of the load cell, extensometer and hoop strain gauges.

3.3. Mechanical behaviour of the aluminium alloy 2017 T4 used for the tests

To validate the above analysis, we ran numerical simulations of the quasi-oedometric compression test of the aluminium. In order to simulate an actual test, the strain hardening law used for the aluminium is the same as that identified in the tensile tests of the reference aluminium (2017 T4). This aluminium has also been used for the specimens of quasi-oedometric compression tests. The curves of axial stress/plastic strain of the two tests were found to superimpose perfectly (Fig. 12). Table 3 shows the parameters of the elastoplastic behaviour obtained from the tests.

3.4. Validation of the method by numerical simulations

A numerical simulation of the quasi-oedometric compression test was run with Abaqus/Explicit (Hibbitt et al., 2003) to check that the method proposed above does reveal the behaviour of the aluminium that was tested. The modelling of the quasi-oedometric test involves large deformations, contacts and non-linear

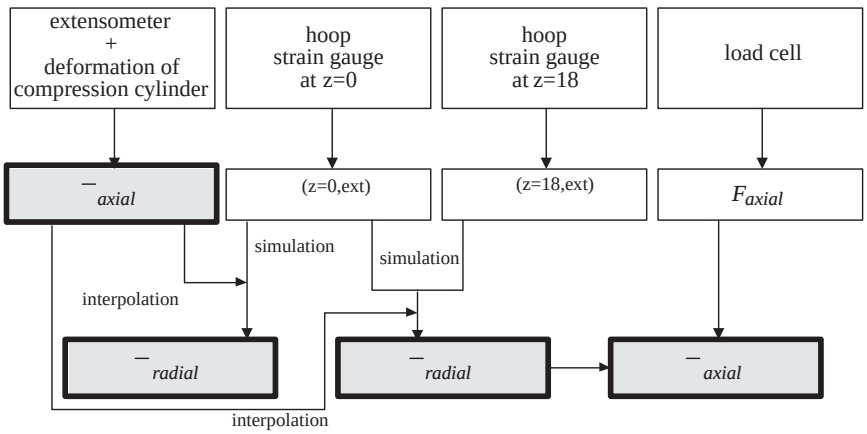

Fig. 11. Outline of the quasi oedometric compression test methodology.

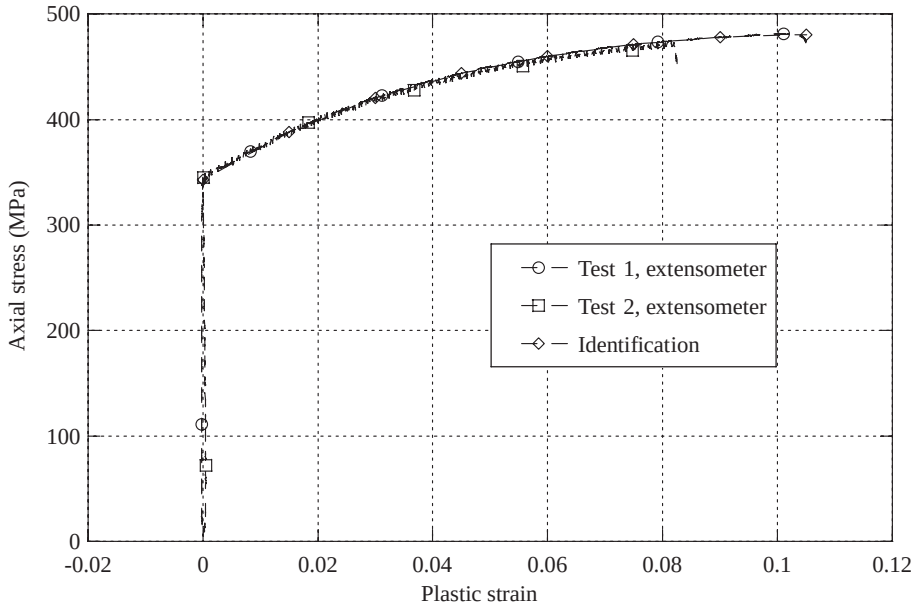

Fig. 12. Strain hardening law for the aluminium alloy 2017 T4 identified from two tensile tests.

Table 3
Parameters of the elastoplastic model used for the aluminium 2017 T4 identified from the tensile tests

Identification of the plastic hardening		
Elastic parameters	E, ν	69 GPa; 0.3
Plastic strain/equivalent stress (MPa)	0	342.6
	0.015	388.2
	0.03	420.7
	0.045	443.8
	0.06	460.0
	0.075	471.2
	0.09	478.1
	0.105	480.5

behaviour of both vessel and specimen materials. The Explicit version of the code was chosen to perform the numerical simulations due to the robustness showed by this code when solving highly non-linear problems. However, the loading rate selected for simulations is small enough to assure the perfect equilibrium of the specimens. Moreover, smaller velocities applied to the upper surface of the specimen did not change the results.

Half the cylindrical specimen was compressed between a steel compression disk and a horizontal plane of symmetry ($z = 0$, Fig. 13). A uniform axial velocity was applied to the upper surface of the compression disk, slow enough to impose a quasi-static loading (this velocity having no influence on the result of the numerical simulation). The steel cylinder was stiff enough to impose a plane axial displacement (Fig. 13b). We used 4-node axisymmetric elements with reduced integration (CAX4R in ABAQUS notation). Prior to any conclusive simulation, some cautions were taken to prevent negative effects of meshing density on the accuracy of the results. Additionally the mesh is finer close to the contact surfaces (see Fig. 13) were localisation of deformations were expected, in order to get a better spatial discretisation, where local effects may appear. Also both kinematic and penalty contact algorithms were previously tested, and master and slave surfaces were switched for every couple of contacting solids; no differences were observed in the numerical results. The axial stress (Fig. 13a) was fairly homogeneous in the specimen (up to 800–900 MPa) but showed a concentration at the level of the contact between the specimen and the pressure disk because the diameter of the specimen is slightly wider. At 15% axial strain, the equivalent Mises stress reaches its maximum level throughout the specimen

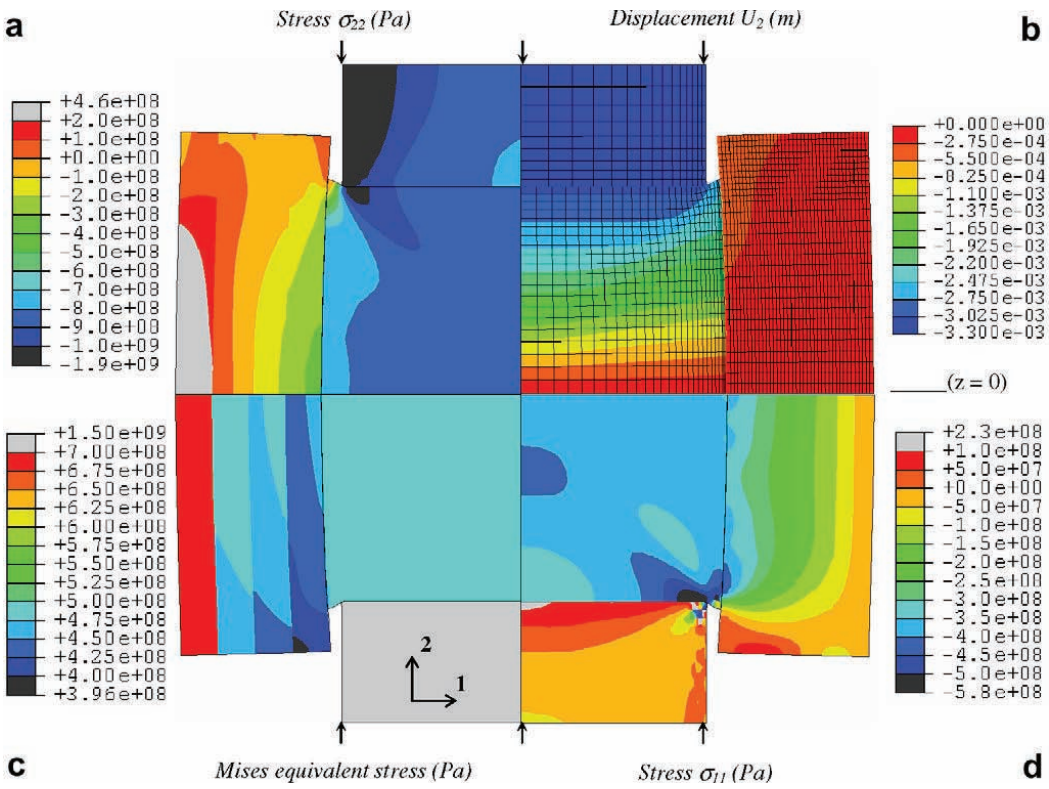

Fig. 13. Numerical simulation of the quasi oedometric compression test (Abaqus/Explicit). (ε_{axial} 15%, zero friction coefficient at contact surfaces).

(480.5 MPa) (Fig. 13c). The radial stress (Fig. 13d) is homogeneous in the specimen and at the level of the specimen/vessel contact, which confirms the hypothesis used in the numerical simulations of Figs. 7 and 8.

Figs. 14–17 present the results of the numerical simulations of the quasi-oedometric compression test of the aluminium alloy which is modeled through an elastoplastic model whose parameters are given in Table 3. The

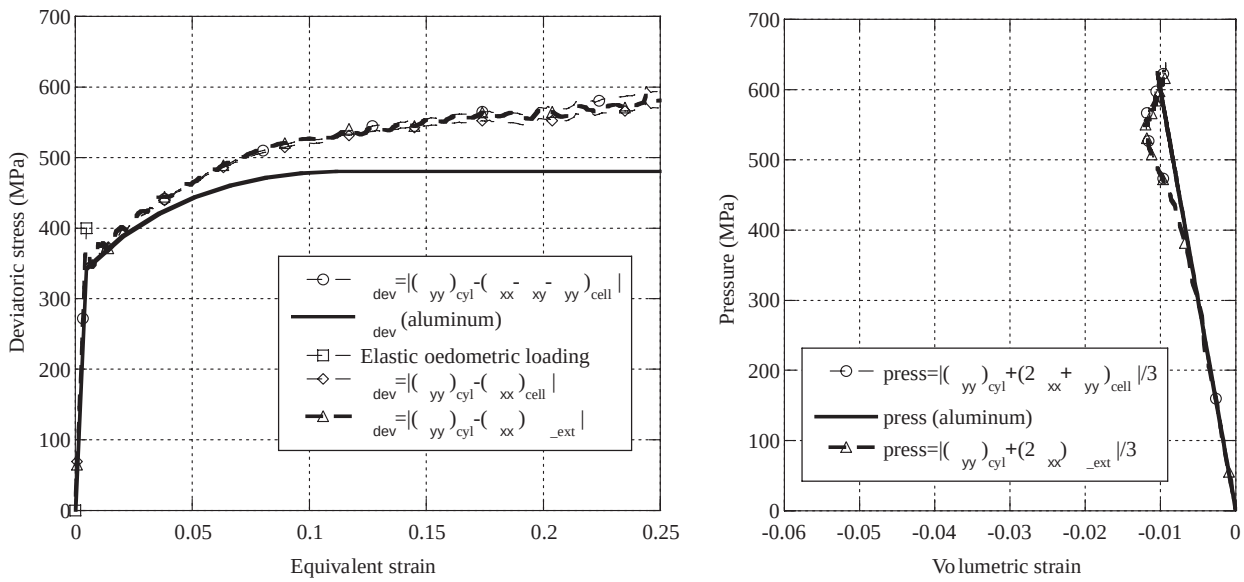

Fig. 14. Numerical simulation of the quasi oedometric compression tests. No friction neither Chrysor® between specimen and vessel. Axial stress by Eq. (16).

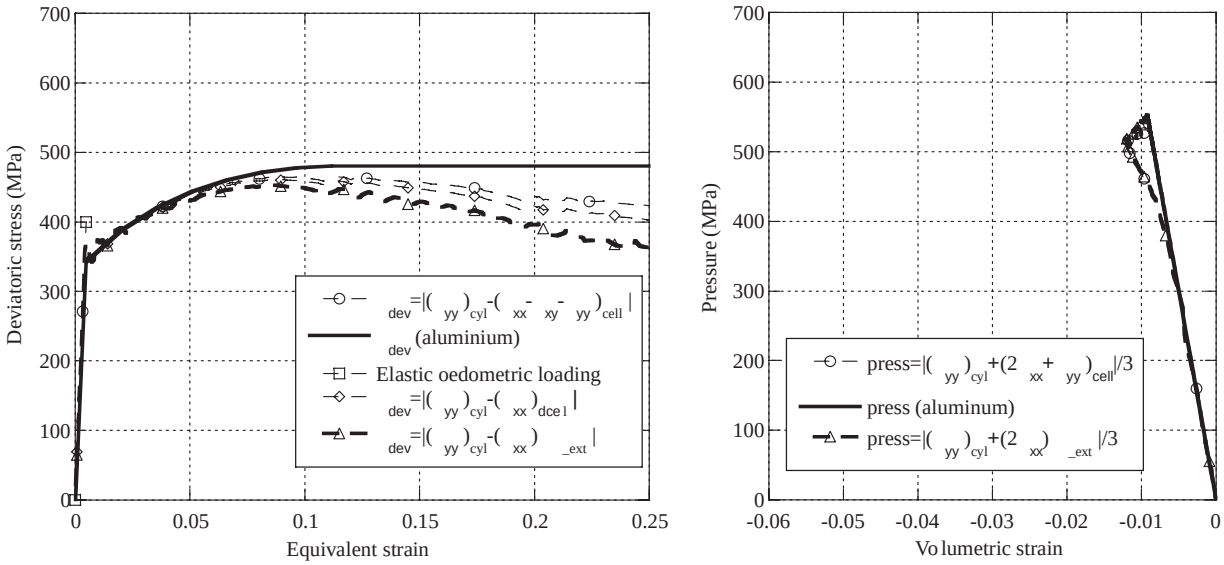

Fig. 15. Numerical simulation of the quasi oedometric compression tests. No friction neither Chrysor® between specimen and vessel. Axial stress by Eq. (17).

left of the Figure shows systematically the deviatoric behaviour (the evolution of the deviatoric stress with the equivalent strain), and the right-hand column the spherical behaviour (the evolution of the hydrostatic pressure with the volumetric strain). The curves with the circular markers correspond to stresses measured from the contact forces given by the numerical simulation:

$$\sigma_{\text{deviatoric}} = \left|\sigma_{\text{axial}} - \left(\sigma^{\text{vessel}}_{\text{radial}}(\vec{F}_n \cdot \vec{x}) - \sigma^{\text{vessel}}_{\text{shear}}(\vec{F}_t \cdot \vec{y}) - \sigma^{\text{vessel}}_{\text{axial}}(\vec{F}_n \cdot \vec{y})\right)\right|, \tag{9}$$

$$P_{\text{hydrostatic}} = -\frac{1}{3}\left(\sigma_{\text{axial}} + 2\sigma^{\text{vessel}}_{\text{radial}}(\vec{F}_n \cdot \vec{x}) + \sigma^{\text{vessel}}_{\text{axial}}(\vec{F}_n \cdot \vec{y})\right), \tag{10}$$

$$\text{with } \sigma^{\text{vessel}} = \frac{F^{\text{vessel}}}{2\pi r_0(1+\varepsilon_{\text{radial}}) \cdot h_0(1+\varepsilon_{\text{axial}})}, \tag{11}$$

with $\vec{F}_n$ and $\vec{F}_t$, respectively, the normal and tangential forces between the specimen and the vessel and $\vec{x}$ and $\vec{y}$ the radial and axial directions. The deviatoric stress takes account of the shear stress $\sigma^{\text{vessel}}_{\text{shear}}$ which occurs only if the vessel exerts friction on the specimen. In the same way, Eqs. (9) and (10) use the axial stress exerted by the vessel on the specimen $\sigma^{\text{vessel}}_{\text{axial}}$, present only if the vessel suffers a barrel deformation. The curves with the rhombus are that of the simplified Equations (12) and (13), which do not take into account the two stresses mentioned above (axial and shear due to barreling and friction). A comparison of both curves shows the extent of the error that would arise from a neglect of the two stresses in the analysis.

$$\sigma_{\text{deviatoric}} = \left|\sigma_{\text{axial}} - \sigma^{\text{vessel}}_{\text{radial}}(\vec{F}_n \cdot \vec{x})\right|, \tag{12}$$

$$P_{\text{hydrostatic}} = -\frac{1}{3}\left(\sigma_{\text{axial}} + 2\sigma^{\text{vessel}}_{\text{radial}}(\vec{F}_n \cdot \vec{x})\right). \tag{13}$$

The curves with triangles are given by the force and the exterior hoop strain of the vessel, as in the analysis of a test

$$\sigma_{\text{deviatoric}} = \left|\sigma_{\text{axial}} - \sigma^{\text{vessel}}_{\text{radial}}(\varepsilon^{\text{ext}}_{\theta\theta})\right|, \tag{14}$$

$$P_{\text{hydrostatic}} = -\frac{1}{3}\left(\sigma_{\text{axial}} + 2\sigma^{\text{vessel}}_{\text{radial}}(\varepsilon^{\text{ext}}_{\theta\theta})\right). \tag{15}$$

The four curves on the left of the Figures and the three on the right help to explain the influence of the successive hypotheses. The distance between the thick continuous line without marks (the behaviour law used for the aluminium) and the one with circles is due to the heterogeneity of the stresses within the volume of the

sample, and this lends weight to the influence of the hypothesis of homogeneous strains in this volume. The separation between the one with circles and that with rhombus shows the importance of the axial stress exerted by the vessel when it adopts a barrel shape, and that of the shear stress of contact (unless there is no coefficient of friction). Unlike the curve with rhombus, the one with triangles uses the radial stress deduced from the exterior hoop strain (Eq. (1), Figs. 7 and 8). The separation between both curves is due to the hypotheses used to construct Eq. (1) (homogeneity of the radial stresses, and a behaviour dependent on the height of application of the pressure but independent of the loading history).

The first three Figs. 14–16 are those of the numerical simulation of a quasi-oedometric compression, assuming zero friction at the contacts and without any interface product. The following numerical simulations (Figs. 14–23) are performed with ABAQUS/Explicit FE code. The axial stress is given by Eqs. (16)–(18).

$$\sigma_{\text{axial}} = \frac{F_{\text{axial}}}{\pi(r_0)^2}, \tag{16}$$

$$\sigma_{\text{axial}} = \frac{F_{\text{axial}}}{\pi(r_0)^2(1+\varepsilon_{\text{radial}})^2}, \tag{17}$$

$$\sigma_{\text{axial}} = \frac{F_{\text{axial}}}{\pi(r_0)^2(1+\varepsilon_{\text{radial}})}. \tag{18}$$

The first two Figs. 14 and 15 reveal an evolution of the equivalent stress far above or far below the expected level (a large separation between the curve with triangles and the continuous one). For example, if one works with Eq. (16) (the nominal axial strain), the equivalent stress is grossly overestimated (an error of about 16% for an equivalent strain of 20%). If the true strain is used (Eq. (17)), the forecast behaviour is correct for an equivalent strain of less than 6 or 7%, whereas the equivalent stress is very much under-estimated beyond this point (roughly 17% error with an equivalent strain of 20%). This error is not due to the evaluation of the radial stress from the exterior strain of the vessel since the same trend is found with the curve with rhomboidal markers that uses the stress given by the specimen/vessel contact force (Eqs. (12) and (13)). The error can only come from a faulty estimation of the axial stress due to the heterogeneity of the axial stress field when the vessel deforms excessively.

Finally, Eq. (18) was used for the diagram of Fig. 16. It allows a determination of the imposed behaviour of the aluminium up to 25% of deviatoric strain. Table 4 shows the error of evaluating the deviatoric stress and

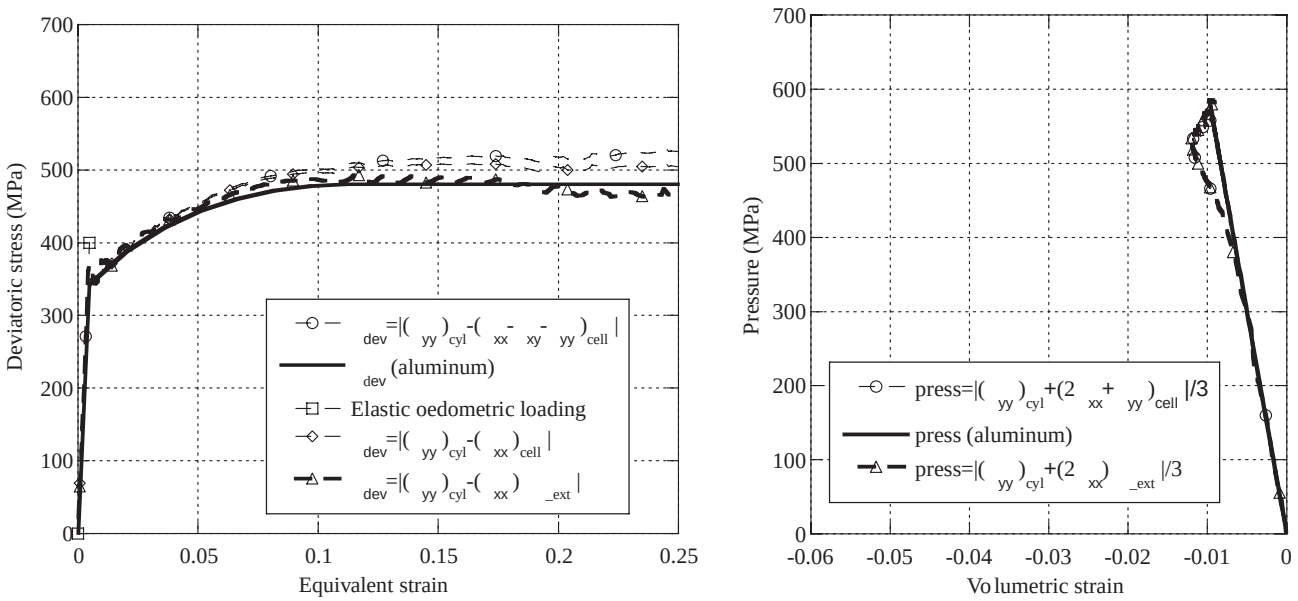

Fig. 16. Numerical simulation of the quasi oedometric compression tests. No friction neither Chrysor® between specimen and vessel. Axial stress by Eq. (18).

Table 4
Difference between the expected behaviour (that of the aluminium alloy) and that measured in Fig. 16 (curve with triangles) for three axial strains

ε_{axial} (%)	$\varepsilon_{\theta\theta}^{(z\ 0,ext)}$(%)	Pressure (MPa)	$\Delta\sigma_{dev.}$ (MPa) (Al Measure)	$\Delta\varepsilon_{volumetric}$ (Al Measure)	Error % ($\sigma_{deviatoric}$)	Error % ($\varepsilon_{volumetric}$)
5	0.8	481	4	0.0023	0.9	28.2
10	1.8	522	9	0.0032	2.0	36.3
20	4.0	563	9	0.0010	1.8	10.2

the volumetric strain. The distance in the deviatoric stress between the curve with triangles (analysis of the simulation) and the imposed behaviour (continuous curve) is of no more than 2% as in Fig. 16 (left-hand side). In the following data analyses we used only Eq. (18).

On the other hand, the error in estimating the spherical behaviour appears more serious (around 36% and 10% for equivalent strains of 10% and 20%). This is explained by the very small volumetric strains showed by the material in the tests. For example, the volumetric strain is about 30 times smaller than the equivalent strain when the axial strain is around −10%. Actually, the absolute error is very slight (for example, 0.0032 at −10% axial strain, Table 4) and much below the volumetric strain of a material normally used in this type of test. By way of comparison, a concrete subjected to a pressure of 560 MPa may easily undergo more than 10% compaction. We turn now to the influence of friction.

3.5. Influence of friction

The following calculation assumes a coefficient of friction of 0.1 between the steel vessel and the specimen. This coefficient has been chosen as a arbitrary value of reference in order to show their influence. According to the numerical simulations, this value leads to an overestimation of the strength that was not observed in the experimental part. So, one may think that this value is an upper limit of the level of friction in the experiments. No interface product is used. The contact between the compression cylinder and the specimen is taken as being frictionless. When the equivalent strain is below 15%, the behaviour measured indirectly from the strains at the steel vessel (curve with triangular markers) is found to overestimate the expected strength of the aluminium (continuous curve) (Fig. 17, left). The difference is equally apparent if one compares the curve with rhombus

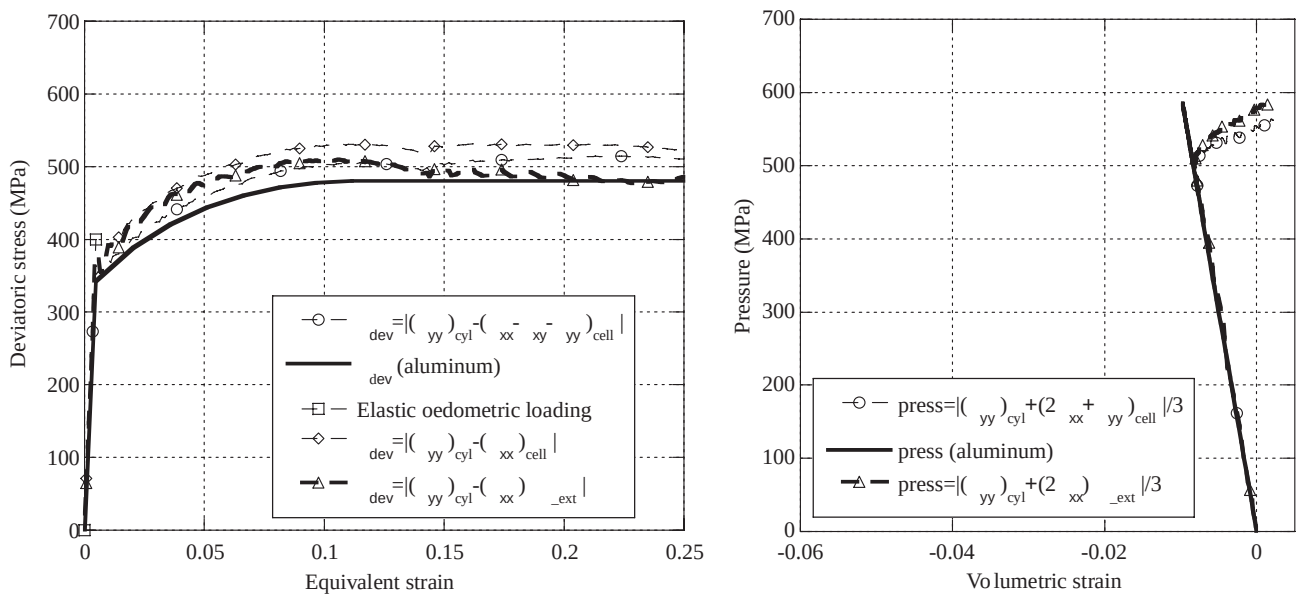

Fig. 17. Numerical simulation of the quasi oedometric compression tests. Friction 0.1 between specimen and vessel, no Chrysor® interface product.

(no consideration of friction, Eq. (12)) and the curve with circles in which friction is taken into account (Eq. (9)). Beyond 15% equivalent strain, the internal radial pressure (Eq. (1)) is overestimated and this compensates the error mentioned above. That is why the error in the deviatoric stress is below 8%. That committed in the spherical behaviour for an axial strain below 10% (in absolute value) is not serious (less than 22%) although beyond that point it increases sharply (Table 5).

3.6. Influence of the Chrysor® interface product

The numerical simulation in Fig. 18 is that of the quasi-oedometric compression of an aluminium specimen of diameter 29.8 mm and height 40 mm.

The vessel still has the original dimensions (interior diameter 30.4 mm, exterior diameter 55 mm, and height 43 mm). The gap of 0.3 mm between the vessel and the specimen is filled in by the Chrysor® interface product that was used in the tests to eliminate any internal gaps. Its properties were identified in tensile tests and under confined compression.

The tensile samples fitted with strain gauges showed a Young's modulus of about 2.2 GPa and a Poisson ratio of 0.28. Confined compression tests were also performed on Chrysor® disks of several thicknesses. These were 60 mm diameter disks placed in a steel confinement cell of 160 mm outer diameter and subjected to uni-

Table 5
Difference between the expected behaviour (of the aluminium alloy) and that measured in Fig. 17 (curve with triangles) for three axial strains

ε_{axial} (%)	$\varepsilon_{\theta\theta}^{(z\ 0,ext)}$(%)	Pressure (MPa)	$\Delta\sigma_{dev.}$ (MPa) (Al Measure)	$\Delta\varepsilon_{volumetric}$ (Al Measure)	Error % ($\sigma_{deviatoric}$)	Error % ($\varepsilon_{volumetric}$)
5	0.9	493	34	0.0001	7.7	1.6
10	2.0	531	30	0.0020	6.2	22.3
20	4.3	573	8	0.0086	1.6	90.3

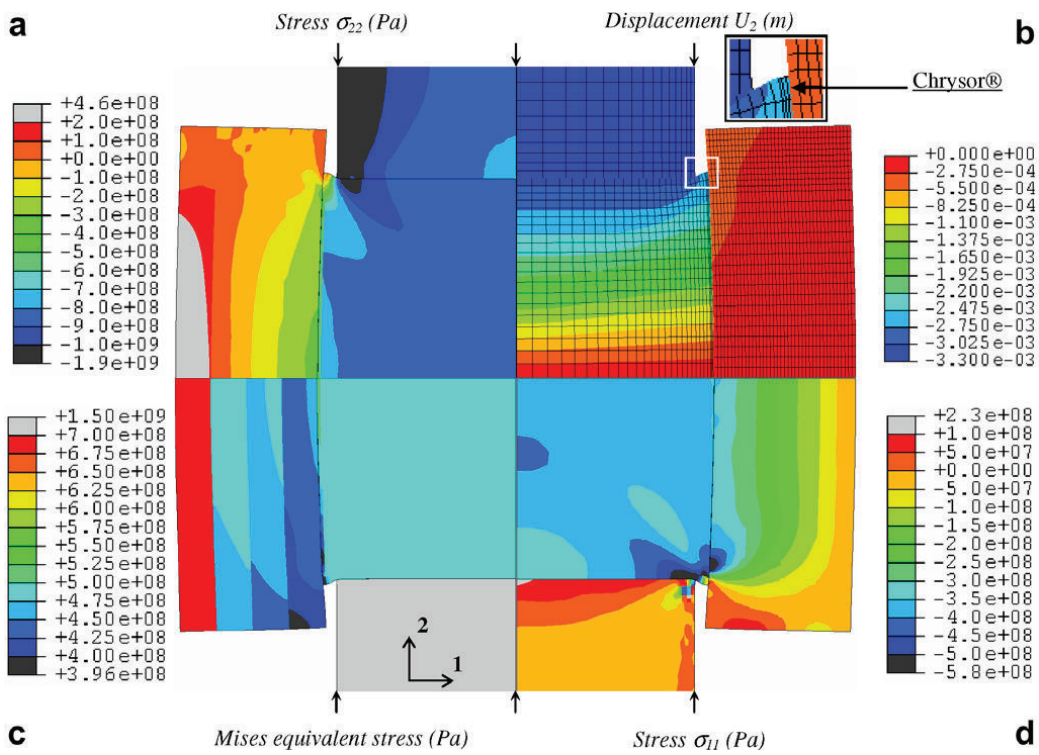

Fig. 18. Numerical simulation of the quasi oedometric test ($\varepsilon_{axial} =$ 15%, friction coefficient nil at contact surfaces).

axial strain. The tests revealed a perfectly elastic behaviour at least up to 300 MPa of axial stress. The apparent elastic modulus M_{apparent} was found to be between 3.8 and 5.3 GPa. The Young's modulus (E) can be deduced, knowing the Poisson ratio (v 0.28), by the equation

$$M_{\text{apparent}}^{\text{elastic uniaxial strain}} = E\frac{(1-2v)(1+v)}{1-v}. \tag{19}$$

The Young modulus was found to be between 3.0 and 4.2 GPa. We used the lower value in the following simulations, considering isotropic elastic behaviour of the interface product. A small extrusion of the Chrysor® during the compression is apparent in Fig. 18. The radial compression stress was wholly transmitted from the specimen to the vessel in spite of the presence of the product (Fig. 18d) and neither did the interface affect the equivalent stress (i.e., von Mises stress) (Fig. 18c). The first numerical simulation (Fig. 19) assumes that friction is nil between the specimen and the vessel and between the specimen and the compression cylinder.

The difference between the deviatoric behaviour imposed and that measured (curve with triangles) is quite small. The fields of the stresses and their evaluation are not affected by the presence of the interface. The volumetric strain is clearly overestimated (in absolute terms) because of an under-estimation of the internal radial strain given by Eq. (2). In fact, part of the radial strain of the specimen is "absorbed" by the crushing and extrusion of the interface product. This is why at −10% axial strain, the error in the volumetric strain is 0.0028 in absolute terms for an internal radial stress of 360 MPa, i.e., an error of about 33% in an aluminium alloy (Table 6).

Fig. 20 gives the analysis of a numerical simulation of quasi-oedometric compression with a friction coefficient of 0.1 at the vessel/specimen interface and it shows that the friction does not modify the deviatoric

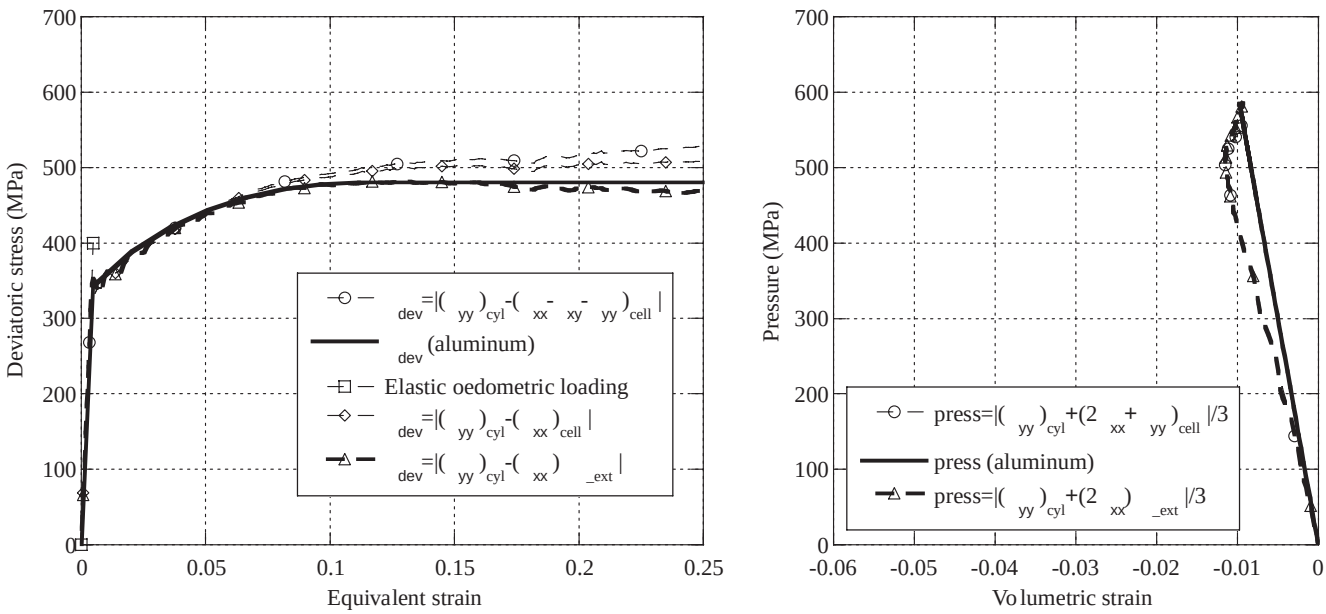

Fig. 19. Numerical simulation of the quasi oedometric compression tests. No friction between solids, Chrysor® interface product between specimen and vessel.

Table 6
Difference between the expected behaviour of the aluminium alloy and that measured in Fig. 19 (curve with triangles) for three axial strains

$\varepsilon_{\text{axial}}$ (%)	$\varepsilon_{\theta\theta}^{(z\ 0,\text{ext})}$(%)	Pressure (MPa)	$\Delta\sigma_{\text{dev.}}$ (MPa) (Al Measure)	$\Delta\varepsilon_{\text{volumetric}}$ (Al Measure)	Error % ($\sigma_{\text{deviatoric}}$)	Error % ($\varepsilon_{\text{volumetric}}$)
5	0.8	473	13	0.0031	2.9	39.3
10	1.8	518	0	0.0028	0.1	33.0
20	3.9	561	11	0.0007	2.2	7.8

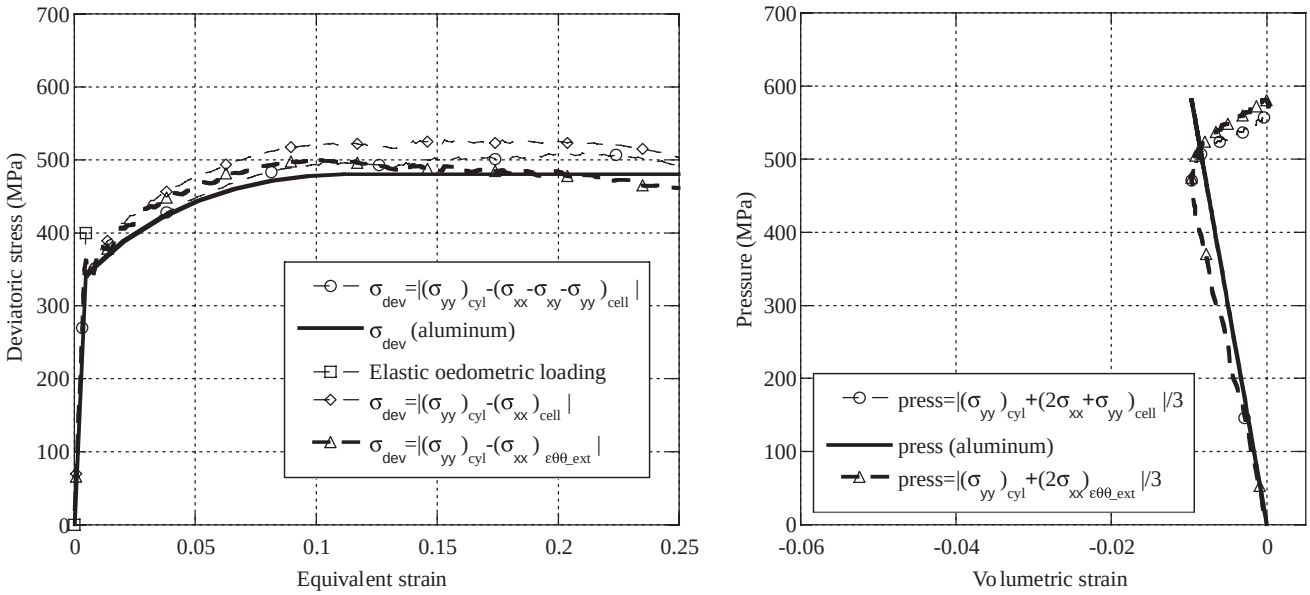

Fig. 20. Numerical simulation of the quasi oedometric compression tests. Friction 0.1 between specimen and vessel, no friction between specimen and compression cylinder, Chrysor® interface product between specimen and vessel.

response in the test. In fact, the difference between the imposed and the observed spherical behaviours is seen to be slightly lower if the axial strain is less than 10% (see Table 7).

The next three Figs. 21–23 give the calculated results of the quasi-oedometric compression of an aluminium specimen, but assuming a gap of 3/10 mm between the compression cylinder plate and the specimen. In the first case (Fig. 21), this gap is completely taken up by the interface Chrysor® whereas it is only partially filled in the second case (Figs. 22 and 23) to take into account a possible void that could remain enclosed during the introduction of the specimen in the vessel (see Section 2). These simulations are intended to detect the effect of a possible defect of parallelism, whether this is compensated or not by the Chrysor® when the specimen is placed in the vessel. In these two cases, the contacts are taken as frictionless. The spherical behaviour is easily predicted but we did find a slight increase of the error; since the interface product deforms under plain strain conditions, its behaviour is still fairly rigid and its presence does not modify greatly the result of the test Tables 8 and 9.

Fig. 22 illustrates the way in which the interface product may cover the gap between the compression cylinder and the specimen. The product is thickest at the centre (3/10 mm) and thinnest at the edges (1/10 mm). The deformation is clearly heterogeneous at the beginning of the compression and then becomes fairly homogeneous. From a certain level of the axial strain, the space between the compression plate and the specimen is filled.

Fig. 23 shows the behaviour obtained with the calculation of Fig. 22. The deviatoric stress is undervalued in the range of weak strain but is as predicted when the equivalent strain is over 5%. For the first time, the spherical strain is seen to be non-linear at weak strain; in a first phase of the compaction, the gap is eliminated between the compression plate and the specimen, and this is followed by a linear increase of the pressure very similar to that of Fig. 19 or Fig. 21. This shows that only the presence of a void between the specimen and the

Table 7
Difference between the expected behaviour of the aluminium alloy and that measured in Fig. 20 (curve with triangles) for three axial strains

ε_{axial} (%)	$\varepsilon_{\theta\theta}^{(\varepsilon\ 0,ext)}$(%)	Pressure (MPa)	$\Delta\ \sigma_{dev.}$ (MPa) (Al Measure)	$\Delta\varepsilon_{volumetric}$ (Al Measure)	Error % ($\sigma_{deviatoric}$)	Error % ($\varepsilon_{volumetric}$)
5	0.8	485	15	0.0014	3.3	17.3
10	1.9	527	22	0.0010	4.5	11.8
20	4.3	570	4	0.0075	0.8	78.6

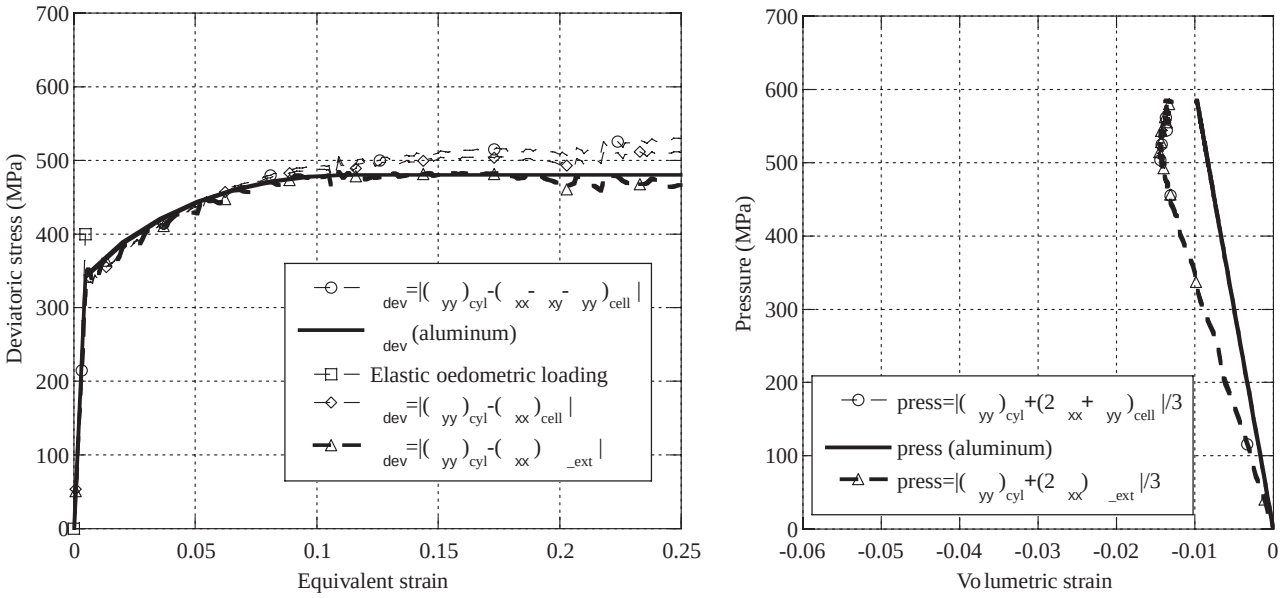

Fig. 21. Numerical simulation of the quasi oedometric compression tests. Chrysor® interface product between specimen and compression cylinder and no friction between these solids.

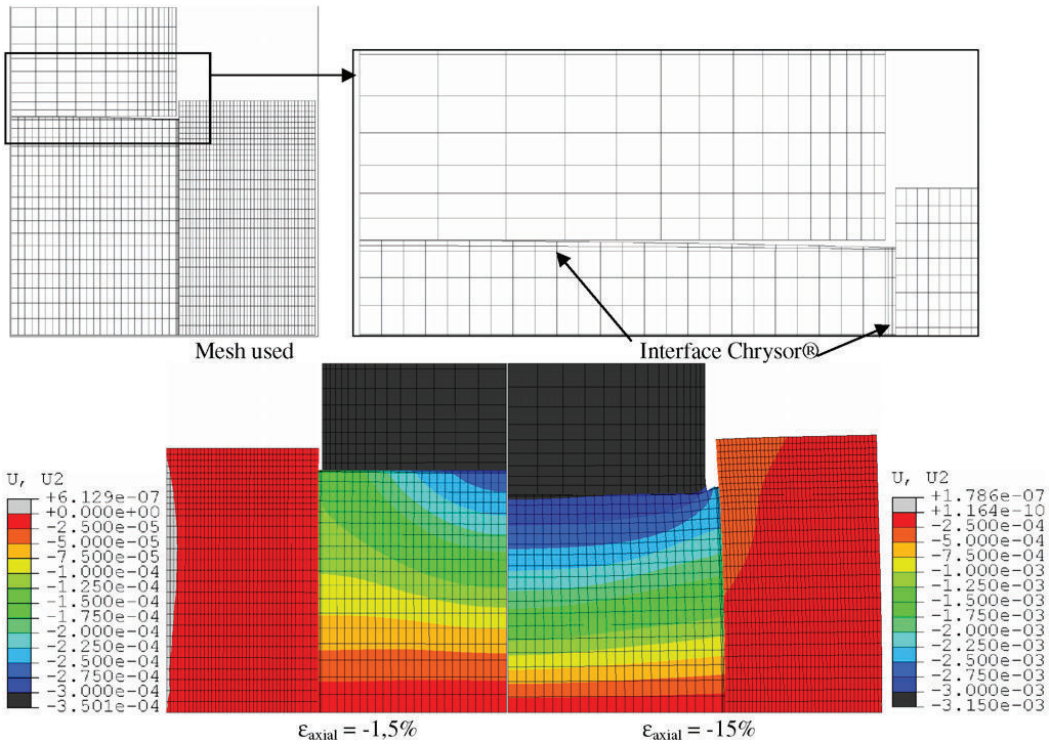

Fig. 22. Numerical simulation of the quasi oedometric compression test. Friction coefficient nil at the contacts, a gap of 3/10 mm between the specimen and the vessel and between the specimen and the compression cylinder).

compression cylinders (or maybe a defect of composition of the Chrysor® interface) may explain that the measured spherical behaviour is found to be non-linear while the behaviour of the material is linear-elastic.

These different numerical simulations provided an evaluation of the qualities and the robustness of the method of analysing the proposed quasi-oedometric compression test. In taking into account the plastic strain of the vessel, it uses the hoop strains measured on the outer surface of the vessel. From this we obtain not only

Table 8
Difference between the expected behaviour of the aluminium alloy and that measured in Fig. 21 (curve with triangles) for three axial strains

ε_{axial} (%)	$\varepsilon_{\theta\theta}^{(z\ 0,ext)}$ (%)	Pressure (MPa)	$\Delta\sigma_{dev.}$ (MPa) (Al Measure)	$\Delta\varepsilon_{volumetric}$ (Al Measure)	Error % ($\sigma_{deviatoric}$)	Error % ($\varepsilon_{volumetric}$)
5	0.7	469	18	0.0056	4.0	71.6
10	1.7	517	1	0.0056	0.2	65.6
20	3.9	561	7	0.0041	1.4	44.2

Table 9
Difference between the expected behaviour of the aluminium alloy and that measured in Fig. 23 (curve with triangles) for three axial strains

ε_{axial} (%)	$\varepsilon_{\theta\theta}^{(z\ 0,ext)}$ (%)	Pressure (MPa)	$\Delta\sigma_{dev.}$ (MPa) (Al Measure)	$\Delta\varepsilon_{volumetric}$ (Al Measure)	Error % ($\sigma_{deviatoric}$)	Error % ($\varepsilon_{volumetric}$)
5	0.6	464	24	0.0097	5.5	126.0
10	1.6	515	1	0.0096	0.3	111.9
20	3.8	564	4	0.0084	0.7	88.9

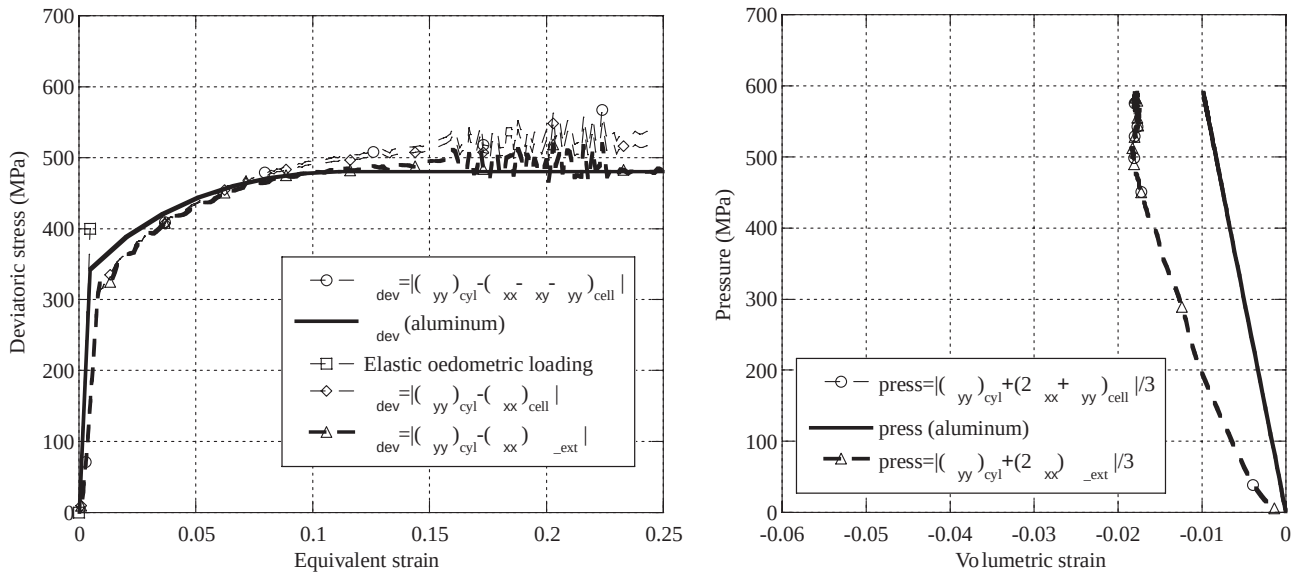

Fig. 23. Numerical simulation of the quasi oedometric compression test. The specimen/vessel interface completely filled in and that between the compression cylinder and the specimen partially filled in by the Chrysor®; no friction at the interfaces.

the internal radial stress and the radial strain of the specimen but also the average axial stress. The simulations show the influence of the experimental conditions (interface friction), the Chrysor® product and any gap between the specimen and the vessel or between the specimen and the compression cylinder.

Friction has a limited influence on the analysis if its coefficient is not above 0.1. Error in the deviatoric stress remains below 8% even if an interface product is used, whereas an error in the volumetric strain is serious if compared to that of the aluminium alloy. This is explained by the low volumetric strain of this material even under a hydrostatic pressure of 600 MPa (ε_v(Al) $\approx -1\%$). For example, this error would be only one-tenth in a concrete, whose volumetric strain is 10 times that of aluminium alloys.

4. Validation of the experimental method by quasi-oedometric compression tests of aluminium specimens

The aim of the quasi-oedometric tests carried out on aluminium was to validate the whole of the experimental set-up and its analysis by using a material whose plastic behaviour is well known and whose mechanical

characteristics under confined compression come as close as possible to those of concrete (except the spherical behaviour). These tests by way of reference ensure the soundness of the method proposed for the analysis of the tests and the accuracy that may be expected in the results. In addition, they expose the difficulties encountered in the experiments, independently of the material behaviour. For this reason, the standard aluminium alloy presented above was used in several quasi-oedometric compression tests; it was chosen on account of its ductility (tensile failure strain above 10%) and of its strength that is close to that of concrete under confined compression (about 500 MPa).

4.1. Experimental method adopted for the tests

Each vessel was chosen for its internal diameter that allowed a crosswise gap (between specimen and vessel) of around 6/10 mm (i.e., 3/10 mm on the radius). A special experimental device was set-up to guarantee very good centering of the vessel, the two compression cylinders and the sample to be tested. First, the steel compression plates are fixed to the platform of the hydraulic machine and their coaxiality is verified. The lower moulding flask centres the lower compression plate in relation to the vessel. Then the vessel is filled to the top with the Chrysor® and the lower flask ensures the necessary watertightness. The specimen, fixed to the upper cylinder with double-sided scotch-tape is directed towards the vessel. The Chrysor® is then extruded through the gap between the vessel and the top compression plate, which has the effect of making the vessel airtight during the operation. Once the specimen touches the lower compression plate, the set-up is left standing for 24 hours before use.

4.2. Results of the quasi-oedometric compression tests of aluminium

In Fig. 24, we see the deviatoric and spherical behaviour observed with the first aluminium specimen 'Al n°1'. This diagram and the following ones also show the familiar elastoplastic behaviour of aluminium (the curve with triangles) as it was identified by the test performed earlier (Fig. 12).

The curve with circles in Fig. 24 on the right shows the evolution of the hydrostatic pressure during the test. In the two first % of strain, the pressure rises very rapidly and then stabilizes between 450 and 550 MPa. So this test looks like a deviatoric strain test under high pressure (of about 500 MPa). A curve with rhombuses (Fig. 24, on the left) gives the theoretical deviatoric elastic behaviour of this aluminium, maintaining the slope up to 300 MPa. If the predicted behaviour is compared now with the aluminium behaviour law, we notice a

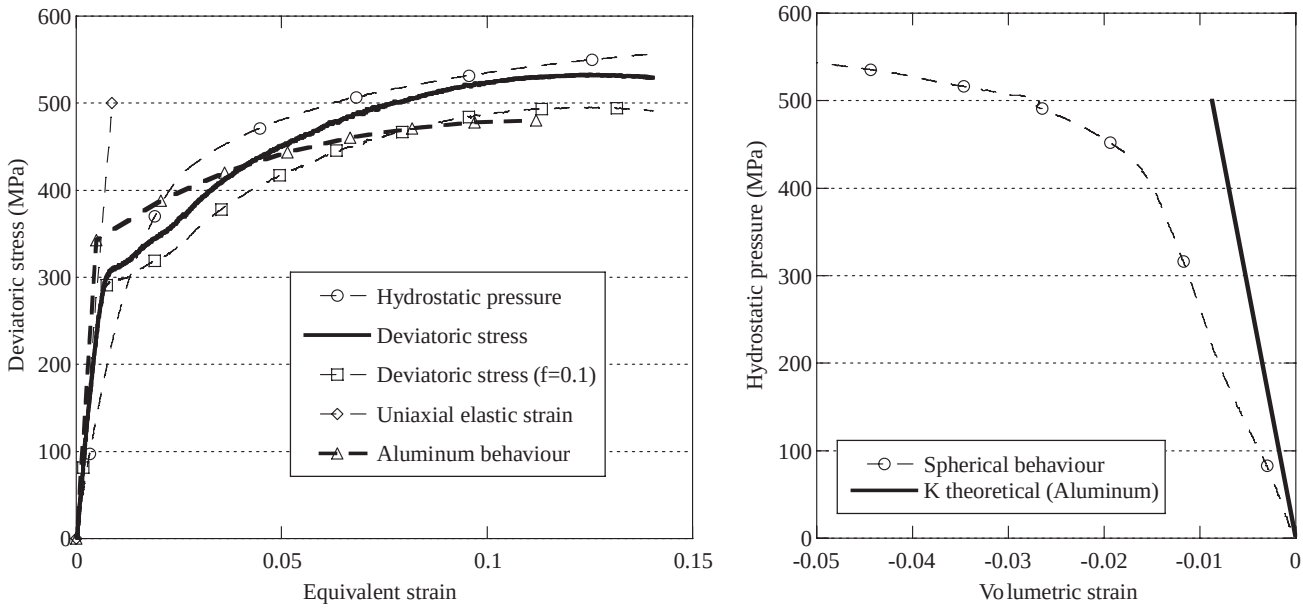

Fig. 24. Results of the quasi oedometric compression tests 'Al n°1'.

slight under-estimation of the plastic behaviour at small strain and a frank over-estimation when the strain rises above 4%. At large strain this could be due to friction between the specimen and the vessel. It is true that when the lateral pressure rises, a fair portion of the axial stress is transmitted to the vessel by the friction, instead of being transmitted to the specimen, and as a consequence the axial stress in the specimen is over-valued. A correction can be made if the coefficient of friction f is known

$$\sigma_{\text{axial}}^{\text{reel}} = \sigma_{\text{axial}}^{\text{apparent}} - f \cdot \sigma_{\text{radial}}. \tag{20}$$

The curve with square markers (Fig. 24, left) presents the response assuming a friction coefficient of 0.1, and this time the strength is not over-estimated at large strains. The evolution of the compaction curve (Fig. 24, right) shows a linear response but with a more gradual slope than that expected from the elastic parameters of aluminium alloy. This behaviour is similar to that of Fig. 21 – (presence of the Chrysor® between the specimen and the vessel and between the specimen and the compression plate but with no void in the vessel). Above a pressure of 450 MPa the measured spherical behaviour diverges, probably because of an over-valuation of the deformation of the specimen due to an extrusion of aluminium outside the vessel.

The next two tests ('A1 n°2' and 'Al n°3') present the following singularity. A Teflon®-type interface product is sprayed onto the inner surface of the vessel before the Chrysor® is put in. And to prevent any extrusion of the anti-adherent Teflon® when the Chrysor® is being extruded, a wide band of scotch-tape is affixed to the Teflon®-treated surface. This tape keeps the Teflon® in place but it also reduces the adherence in the course of the confined compression. The result of these tests is given below. One can see that although the strength is slightly under-valued at weak strain, it is predicted accurately when the strain is over 5%. The volumetric strain, however, is clearly over-valued. This time the curves (Figs. 25 and 26) are closer to the simulation in Fig. 22. A small void in the vessel could explain a slight underestimation of strength at weak strain (Fig. 23), however, this effect is not able to explain the entire underestimation of equivalent stress. It may be explained also by the stepped variation of the mechanical properties of the vessel in the numerical model. Furthermore, at the end of test Al n°3 the volumetric strain is under-valued (in absolute terms), probably because of an undervaluation of the axial strain as a consequence of a small rotation of the extensometer that was noticed at the end of the test.

The singularity of test Al n°4 is that no Chrysor® interface was used. The aluminium specimen was forced into the vessel. Before this, the specimen diameter along its whole height was 30.12 mm, while the interior diameter of the vessel was 30.10 mm. The deviatoric behaviour is reasonably predicted to be frictionless. The spherical behaviour reproduces, again reasonably well, the bulk modulus of the aluminium. There was

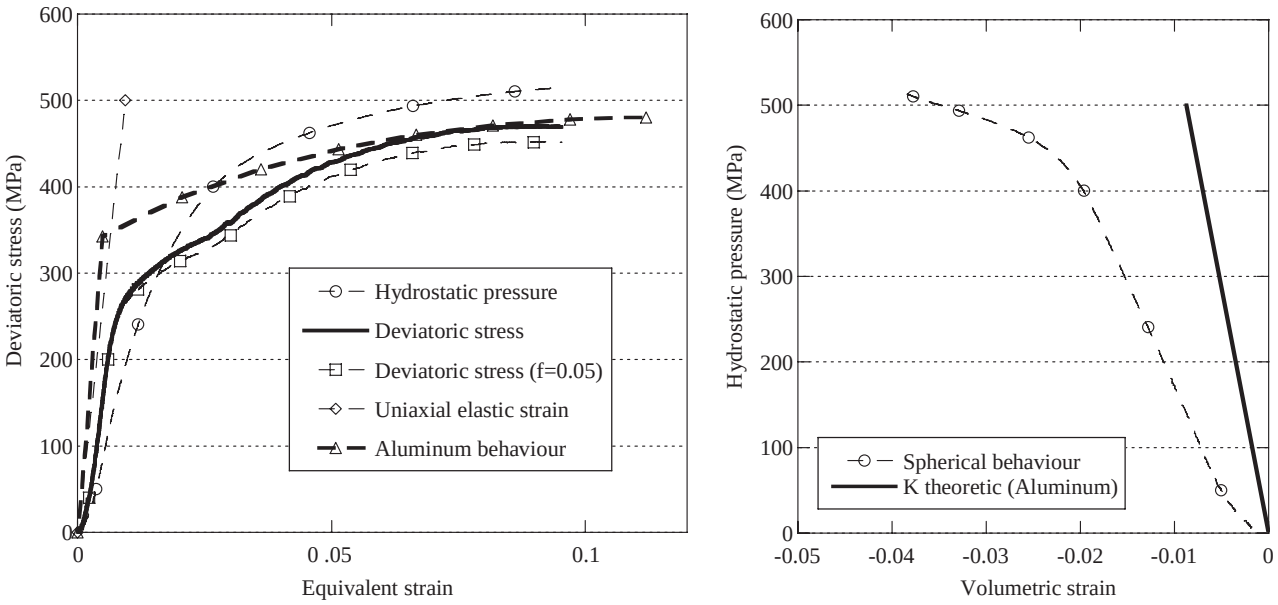

Fig. 25. Results of the quasi oedometric compression tests 'Al n°2'.

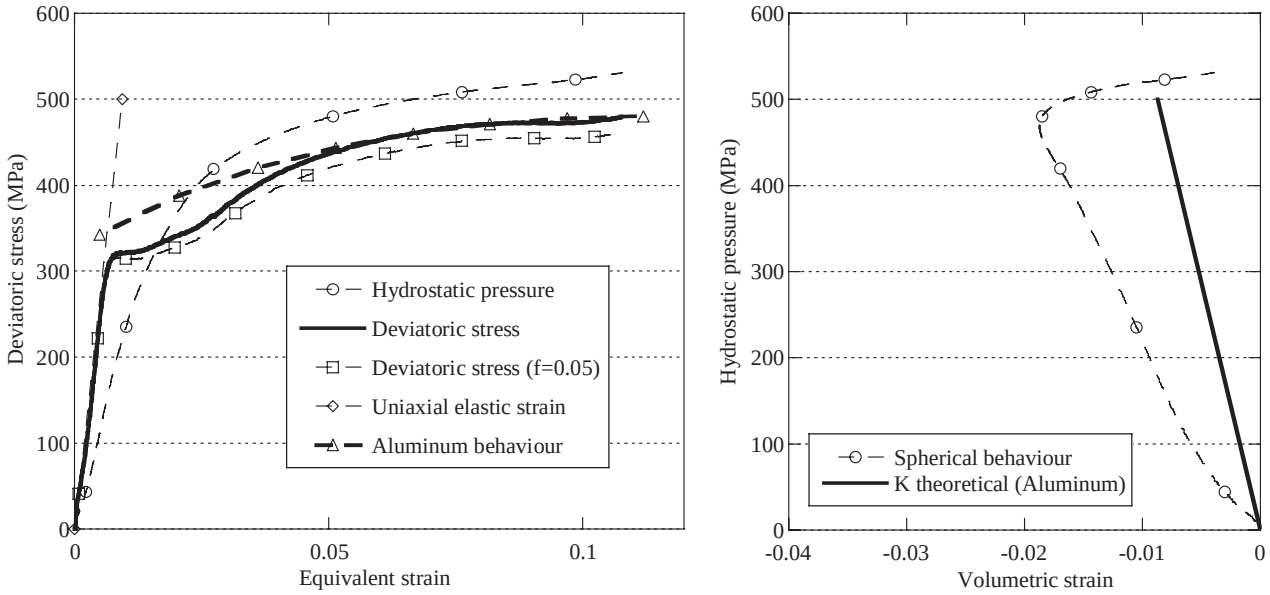

Fig. 26. Results of the quasi œdométric compression tests 'Al n°3'.

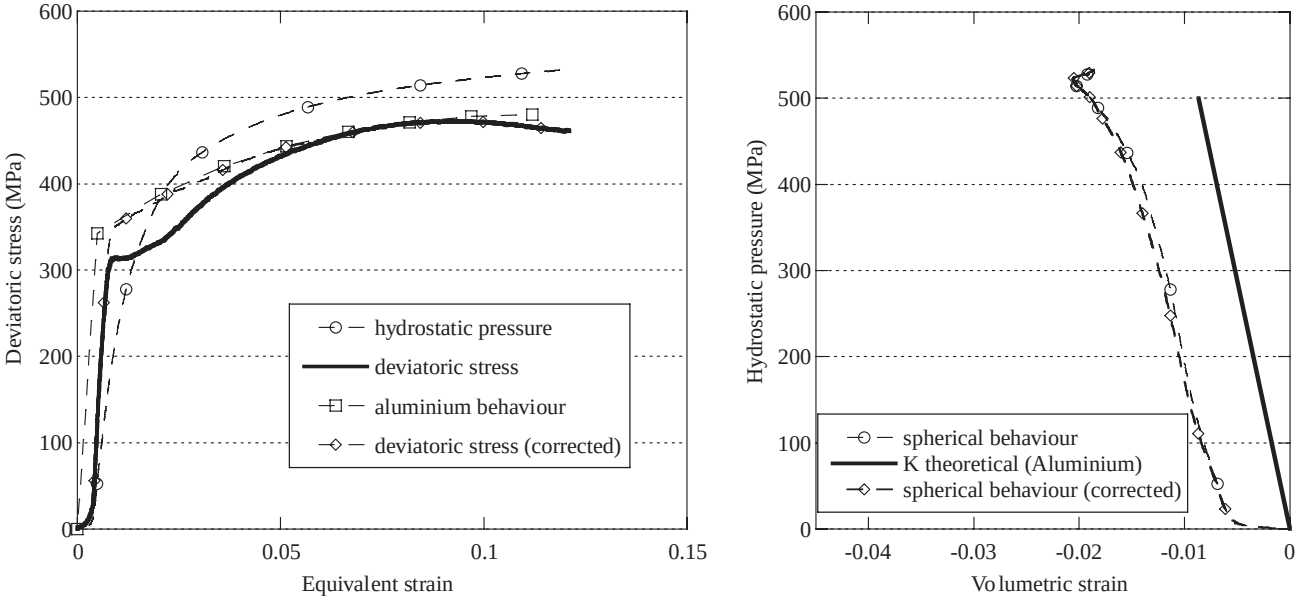

Fig. 27. Results of the quasi oedometric compression tests 'Al n°4'.

a difference, however, of 0.5% between the volumetric strain and the expected elastic behaviour. This discrepancy is an effect of the rise of the axial strain observed at the beginning of the test and not expressed as an increase of the axial stress. A minimum movement of the compression cylinders at the start of the test could explain this phenomenon.

Beyond the specific peculiarities of each test, they revealed a systematic underestimation of the equivalent stress at weak strain, supposedly due to the complexity of evaluating accurately the true field of mechanical properties of the vessel (variation of strength versus radius). Therefore, the relation between hoop stress in the vessel and internal radial stress (Eq. (1)) has been corrected to fit the stress-strain curve obtained with the quasi-oedometric test Al n°4 to the reference curve of the aluminium. The result of the new treatment is visible on Fig. 27. As expected, the equivalent stress/strain curve is superposed to the reference curve

and the evolution of pressure with the volumetric strain has not changed. This correction, which represents less than 12% of the value of radial stress in Eq. (1), allowed obtaining a more reliable result of the strength versus pressure behaviour of the concrete.

5. Quasi-oedometric compression tests of a cement based material containing or not alumina particles

Two materials were prepared and tested under quasi-oedometric compression. The first, called M2 (Fig. 28) is a mortar with no reinforcement, composed of fine sand (of average grain size ≈300 μm, maximum size ≈500 μm), Lafarge cement (PEMS 52.5), silica fume, water and additive. Mix proportions are detailed in Table 10. The microstructure obtained was that of a very fine grain, much smaller than that of the alumina particles added in the second type of material. The mass ratio water/binder (cement + silica fume) is around 0.41, and the ratio sand/binder was 2.2. This composition gives a satisfactory relation between production

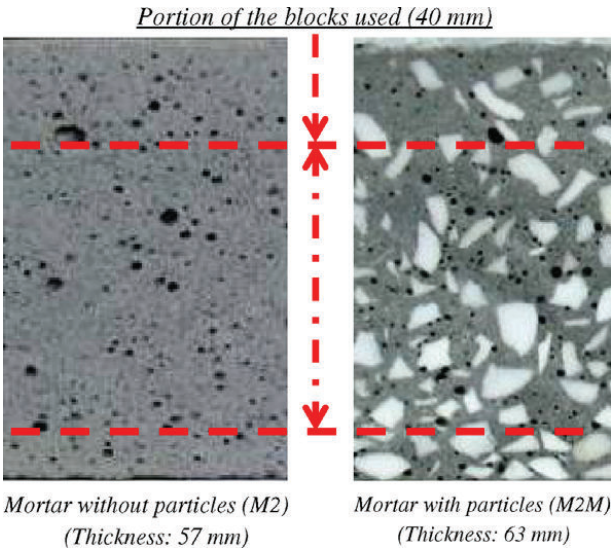

Fig. 28. Surface of a portion of cut blocks for both types of mortar.

Table 10
Elementary properties of the two mortars

Parameters	Mortar M2	Mortar M2M
Mix proportions (kg/m^3)		
Sand (quartz)	1332	941.5
Silica fume	55.5	39.2
Cement	555	392.3
Water	253	178.9
Admixture	4.6	3.3
Alumina particles		1084.4
Water/(cement + silica fume)	0.41	0.41
Sand/(cement + silica fume)	2.2	2.2
Silica fume/cement	0.1	0.1
Mass fraction of particles		0.412
Three point bending tests		
Average strength (σ_w)	8.9 MPa	9.24 MPa
Number of specimens	22	12
Simple compression tests		
Average strength	67 MPa	71 MPa
Number of specimens	4	2

cost, malleability and strength. The second type of mortar, the M2M, (Fig. 28) had the same composition as the first – fine sand, cement, silica fume, water, additive – with the addition of the angular alumina particles (41.1% by mass, around 30% vol.) of medium size (3–6 mm) obtained by sintering and subsequent crushing. The concrete pastes were prepared with a 40 l capacity mixing machine and poured into plywood moulds that had not been submitted to vibration to avoid any accumulation of the ceramic particles in the lower part of the moulds. The materials were stored in airtight container at room temperature at least 28 days before opening.

The cylindrical and cubic samples used in the study were cut and extracted from the interior of two large blocks (around $280 \times 200 \times 60$ mm^3), one from each mortar. The samples were cut at more than 10 cm from the surface of the blocks so each one was considered homogeneous and not dependent on the zone in the block from which it was taken. Fig. 28 shows the surface of a portion of a cut block. The porosity appears to be homogeneous and the distribution of the particles is fairly especially in the part of the blocks used.

Elementary properties of the two mortars, M2 and M2M are shown in Table 10. A first estimate gives the density of the matrix (ρ_{Mi}) of the mortar with particles M2M (ρ_{M2M} 2.61) from the mass fraction of the particles used (f_{mP} 41.1%) and the density of the particles of alumina (ρ_{P} 3.58) (Eq. (21)).

$$\rho_{\mathrm{Mi}} = (1 - f_{\mathrm{mP}})\left[\frac{\rho_{\mathrm{Ci}}\rho_{\mathrm{P}}}{\rho_P - f_{\mathrm{mP}}\rho_{\mathrm{Ci}}}\right]. \tag{21}$$

The calculated density of the matrix (ρ_{M} 2.195) is almost the same as that of the mortar type M2 (ρ_{M2} 2.18). The porosity of the matrix of the M2M is of the same order of that of the M2. Three-point bending tests were done with cubic samples measuring $100 \times 20 \times 15$ mm^3. Twelve tests were done with the type M2M and 22 with the M2. Since the average failure stresses are very similar for the two mortars, it would seem that the addition of the particles does not lessen the strength of the M2M. Simple compression tests were also performed. Cylindrical samples of 30 mm diameter and 40 mm in length were cut from cement blocks with a diamond cutter. The end surfaces were then cut, rectified and polished. The average failure strengths measured were 67 MPa with the M2 mortar and 71 MPa with the M2M material. The particles, as in three-point bending, did not modify the average strength.

The deviatoric and spherical curves of the two mortars M2 and M2M under confined compression are shown in Fig. 29. A notable rise of strength occurs with the hydrostatic pressure. While the simple compression strength of the M2 mortar is about 67 MPa, it rises to over 150 MPa under a hydrostatic pressure of

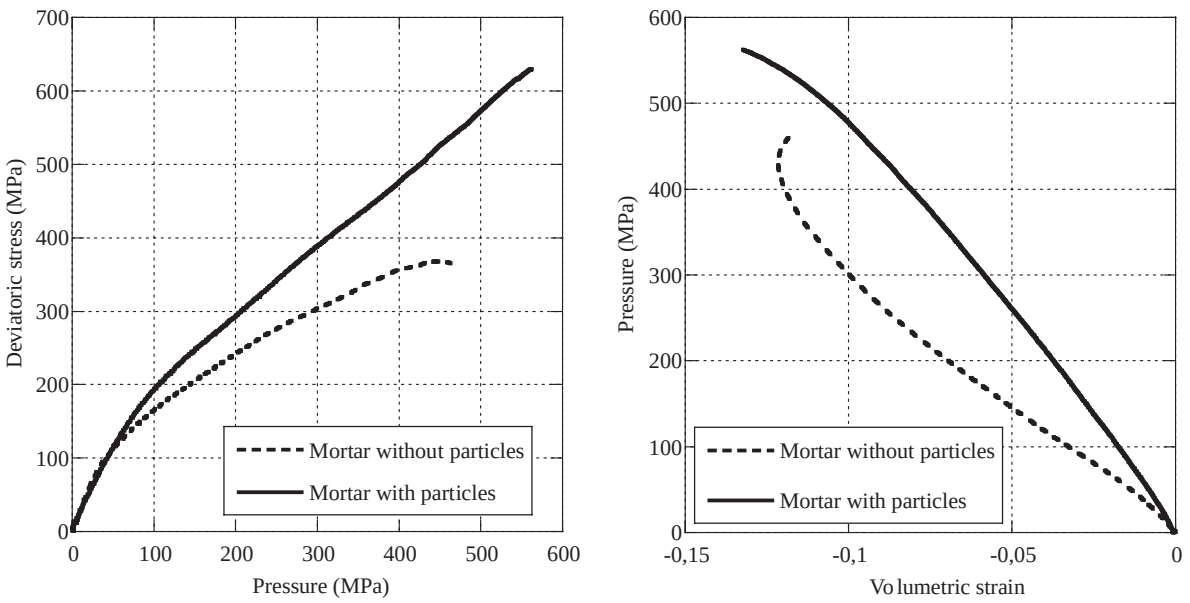

Deviatoric behaviour: evolution of the strength with hydrostatic pressure

Spherical behaviour: evolution of the volumetric strain with hydrostatic pressure

Fig. 29. Deviatoric and spherical behaviours of mortars M2 and M2M.

80 MPa and is even reaching 368 MPa under a hydrostatic pressure of 450 MPa. The rise of strength of the reinforced type M2M is even more spectacular than that of the M2. Under light confinement ($P_{\text{hydrostatic}}$ 80 MPa, strength 164 MPa) it is similar, but it is 30% higher than that of the M2 under strong confinement and reaches 630 MPa under a hydrostatic pressure of 560 MPa. So the addition of particles of alumina has a very beneficial effect on the strength of the mortars under high confining pressure. The compaction curves reveal a marked reduction of volume under these high pressures. The volume of the M2 specimens is reduced by about 12% under a load of 400 MPa, while it is below 8.1% in the M2M under the same load. Again the presence of the particles is seen to be highly beneficial since the compaction of the mortar with particles is reduced. This result may be explained easily by the fact that compaction (likely due to pore collapse) is focused on the matrix, pressure being too low to allow any compaction of alumina particles.

6. Conclusion

This work presents a new method of analysis of the quasi-oedometric compression test. It uses the hoop strains measured on the outer surface of the vessel together with axial force given by the load cell and the axial strain furnished by the extensometer. From these experimental data we deduce the internal radial stress, the radial strain of the specimen. The originality of the method is to take into account on one hand the plastic and 'barrel' deformation of the vessel and on the other hand the axial contraction of the sample to predict as accurate as possible the radial stress and strain evolutions of the specimen. Then, it is possible to evaluate the spherical and deviatoric behaviour of the sample material.

Moreover, various numerical simulations were performed to provide an estimation of the qualities and the robustness of the method of analysis. From these simulations we evaluated the influence of the experimental conditions: interface friction at contact surfaces, the Chrysor® resin filling the specimen–vessel or specimen–compression cylinder interfaces, or any void at these interfaces. Friction has little influence on the data analysis if the friction coefficient is below 0.1. The error committed with the deviatoric stress does not pass 8%, even when an interface product is used. The calculations also predict a maximum error in the volumetric strain, of the order of 0.005–0.01 depending on the use or non-use of an interface product. This error is inadmissible if it is a question of measuring the modulus of compressibility of an aluminium alloy, but it does not go above 5–10% of the volumetric strain of a concrete subjected to a pressure of 600 MPa, similar to the error that might be made with the deviatoric strength.

The four quasi-oedometric compression tests performed with a reference material (aluminium specimens) provided a scanning and almost a validation of the method of analysis and of the experimental protocol. As suggested by the curves of the deviatoric behaviour, the use of a non-stick product with a band of scotch-tape in addition to the interface product does away with any friction between the vessel and the specimen. An underestimation of the deviatoric strength, of the order of 40–60 MPa may occur at the beginning of the test, as well as an overvaluation of the compaction of around 0.005–0.01. This experimental method may be used to analyse the behaviour of geomaterials under confined compression.

Acknowledgements

The authors are indebted to the Spanish Comisión Interministerial de Ciencia y Tecnología (Project MAT2002-03339) for the financial support of this work and to the Délégation Générale pour l'Armement (DGA/France) for the mobility Grant provided to Dr. Forquin.

References

Bažant, Z.P., Bishop, F.C., Chang, T.P., 1986. Confined compression tests of cement paste and concrete up to 300 ksi. ACI J. 33, 553 560.

Bažant, Z.P., Xiang, Y., Adley, M.D., Prat, P.C., Akers, S.A., 1996. Microplane model for concrete. II: data delocalization and verification. J. Eng. Mech. 122 (3), 255 262.

Burlion, N. 1997. Compaction des bétons: éléments de modélisation et caractérisation expérimentale. Ph.D. dissertation, Ecole Normale Supérieure de Cachan, France.

Burlion, N., Pijaudier Cabot, G., Dahan, N., 2001. Experimental analysis of compaction of concrete and mortar. Int. J. Numer. Anal. Methods Geomech. 25, 1467 1486.

Buzaud E., 1998. Performances mécaniques et balistiques du microbéton MB50, DGA/Centre d'Etudes de Gramat. Report.
Cagnoux, J., Don, D., 1994. Compressions uniaxiale, hydrostatique et triaxiale du quartzite de Villejust et du calcaire de Montmoyen. T 94 38, DGA/Centre d'Etudes de Gramat. Report.
Forquin, P., 2003. Endommagement et fissuration de matériaux fragiles sous impact balistique, rôle de la microstructure. Ph.D. dissertation, Ecole Normale Supérieure de Cachan, France.
Gatuingt, F., 1999. Prévision de la rupture des ouvrages en béton sollicités en dynamique rapide. Ph.D. dissertation, Ecole Normale Supérieure de Cachan, France.
Hanchak, S.J., Forrestal, M.J., Young, E.R., Ehrgott, J.Q., 1992. Perforation of concrete slabs with 48 and 140 MPa unconfined compressive strength. Int. J. Impact Eng. 12 (1), 1 7.
Heard, H.A., Cline, C.F., 1980. Mechanical behaviour of polycrystalline BeO, Al2O3 and AlN at high pressure. J. Mater. Sci. 15, 1889 1897.
Hibbitt, H.D., Karlsson, B.I., Sorensen, P., 2003. Abaqus User's Manual, ABAQUS/IMPLICIT. Version 6.1.
Hoek, E., Franklin, J.A., 1968. Simple triaxial cell for field or laboratory testing of rock. Trans. Inst. Min. Metall. 77, A22 (Section A).
Kolsky, H., 1949. An investigation of mechanical properties of materials at very high rates of loading. Proc. Phys. Soc. Lond. B 62, 676 700.
Kotsovos, M.D., Newman, J.B., 1980. Mathematical description of deformational behavior of concrete under generalized stress beyond ultimate strength. J. Am. Concr. Inst. ACI 77, 340 346.
Palaniswamy, R., Shah, S.P., 1974. Fracture and stress strain relationship of concrete under triaxial compression. J. Struct. Div., ASCE, ST5, 901 916.
Wallace, G., Olden, O.J., 1965. Foundation testing techniques for arch dams and underground developments. ASTM, STP, 402.
Xie, J., Elwi, A.E., MacGregor, J.G., 1995. Mechanical properties of three high strength concretes containing silica fume. ACI Mat. J. 92 (2), 135 145.
Xu, Y., Keer, L.M., Luk, V.K., 1997. Elastic cracked model for penetration into unreinforced concrete targets with ogival nose projectiles. Int. J. Solids Struct. 34 (12), 1479 1491.
Yankelevsky, D.Z., Dancygier, A.N., 2001. Uniaxial compressive strength effect on high velocity penetration into thick NSC and HSC targets. Symposium ISIEMS.